Carbohydrate Polymers 390 (2026) 125726

Contents lists available at ScienceDirect

Carbohydrate Polymers

journal homepage: www.elsevier.com/locate/carbpol

Preferential solvation drives polysaccharide conformation and viscoelasticity

Pallab Kumar Borah [a,b,*], Joshua E.S.J. Reid [b], Thomas MacCalman [c], Amir H. Irani [d,e], Daniela Russo [f], Jens Smiatek [g], Johannes Hunger [h], Mona Sarter [i], Vlad Dinu [c], Francesca Natali [f], Michael Boehm [j], Stephen E. Harding [c], Martin A.K. Williams [k], Stefan K. Baier [j,l], Gleb E. Yakubov [b,m,**]

[a] Heinz Maier-Leibnitz Zentrum, Technical University of Munich, Lichtenbergstraße 1, 85748, Germany
[b] Food Materials Research Group, School of Biosciences, University of Nottingham, LE12 5RD, United Kingdom
[c] National Centre for Macromolecular Hydrodynamics, University of Nottingham, LE12 5RD, United Kingdom
[d] Department of Anaesthesia, Te Whatu Ora, Waikato Hospital, Hamilton, 3204, New Zealand
[e] School of Science and Arts, American International University, Jahrah, 13034, Kuwait
[f] CNR-Istituto Officina dei Materiali and INSIDE@ILL, Institut Laue Langevin, Grenoble, 38042, France
[g] Institute for Computational Physics, University of Stuttgart, Allmandring 3, Stuttgart, 70569, Germany
[h] Department of Molecular Spectroscopy, Max Planck Institute for Polymer Research, Mainz, 55128, Germany
[i] ISIS Neutron and Muon Source, STFC Rutherford Appleton Laboratory, Didcot, OX11 0QX, United Kingdom
[j] Motif FoodWorks Inc., 27 Drydock Avenue, Boston, MA, 02210, United States of America
[k] School of Fundamental Sciences, Massey University, Palmerston North, 4442, New Zealand
[l] School of Chemical Engineering, University of Queensland, Brisbane, QLD, 4072, Australia
[m] Food Colloids and Bioprocessing Group, School of Food Science and Nutrition, University of Leeds, Leeds, LS2 9JT, United Kingdom

ARTICLE INFO

Keywords:
Polysaccharide conformation
Preferential solvation
Viscoelasticity
Pectin
Water-glycerol mixtures
Neutron scattering

ABSTRACT

Polysaccharide conformations are central to biological function but exhibit a strikingly counterintuitive, non-monotonic behaviour. Addition of a poorer cosolvent, such as glycerol, to aqueous polysaccharide solutions induces flexible coil → swollen → collapsed conformational transitions as the solvent quality becomes progressively poorer. Using complementary simulations, theory, and experiments, we show that preferential solvation governs the conformational transitions, where the distribution of solvent molecules around the polysaccharide chain deviates significantly from that in the bulk solution. Contrary to expectations, initial chain swelling arises from preferential binding of glycerol at lower glycerol volume fraction, whereas preferential hydration leads to a more compact (collapsed) configuration at higher glycerol volume fraction. Chains appear to conserve their total water contact via such conformational reconfigurations, which map directly onto viscoelastic response; a phenomenon that may be greatly accentuated in polysaccharides. Results are explained from the perspective of Kirkwood-Buff solution theory and solvent entropic penalties, which extend beyond the Flory-type mean-field description. A tentatively unified behaviour can be observed across complex polysaccharides, including pectin, as well as other linear and branched polysaccharides such as agar, alginate, carboxymethylcellulose, and dextran, suggesting potential fundamental significance for biological and industrial aspects of glycoscience.

1. Introduction

Polysaccharides are the most abundant class of natural macromolecules and, together with nucleic acids, proteins, and lipids, constitute the four fundamental building blocks of life (Marth, 2008). Structurally, they are long-chain carbohydrate polymers composed of

* Correspondence to: P. K. Borah, Heinz Maier-Leibnitz Zentrum, Technical University of Munich, Lichtenbergstraße 1, 85748, Germany.
** Correspondence to: G. E. Yakubov, Food Colloids and Bioprocessing Group, School of Food Science and Nutrition, University of Leeds, Leeds, LS2 9JT, United Kingdom.
E-mail addresses: Pallab.Borah@tum.de (P.K. Borah), G.Yakubov@leeds.ac.uk (G.E. Yakubov).

https://doi.org/10.1016/j.carbpol.2026.125726
Received 5 May 2026; Received in revised form 12 July 2026; Accepted 3 August 2026
Available online 4 August 2026

monosaccharides linked together by glycosidic bonds and exhibit remarkable structural diversity, ranging from linear chains to highly branched architectures with varied three-dimensional topologies and conformations (Gericke et al., 2024). This diversity underpins an equally broad set of biological functions. In plants, for example, cellulose and hemicellulose confer mechanical integrity to cell walls, and pectin plays a crucial role in cell-cell adhesion and cellular signalling, including the activation of membrane receptors (Berglund et al., 2020; Haas et al., 2020; Wachsman et al., 2020). In carnivorous plants, highly viscoelastic, acidic mucilage facilitates the capture of prey, while chitin forms the exoskeleton of arthropods (Freund et al., 2022; Sabbadin et al., 2018). And across all life forms, polymeric glycans of the glycocalyx, a carbohydrate-rich layer surrounding cell surfaces, and a variety of glycosaminoglycans are key regulators of cell signalling, adhesion, and immunomodulation (Bernal-Bayard et al., 2023; Le Pennec et al., 2024; Spellmon et al., 2022). Such biological processes typically occur in aqueous environments, and water is regarded as a good solvent for complex polysaccharides, in which the chains adopt the so-called flexible, coil-like conformation (Alba et al., 2018; Antoniou & Alexandridis, 2010). However, cellular environments are seldom purely aqueous. Several living organisms, including microalgae, plants, fish, insects, and fungi, accumulate cosolvents such as glycerol in micromolar to molar concentrations (de Jong et al., 1997; Ditlecadet et al., 2010; Finn et al., 2015; Raymond et al., 2020; Toxopeus et al., 2019; Zhao et al., 2019). Beyond its central biological relevance, glycerol is widely employed in industrial processes and is generally regarded as a poorer cosolvent for polysaccharides compared to water, in which chains tend to adopt a more compact (collapsed) configuration (Antoniou & Alexandridis, 2010; Jimenez et al., 2022).

A recurrent but unresolved observation is that complex polysaccharides undergo non-monotonic conformational transitions in miscible heterogeneous solvents of water and glycerol. For example, low accumulation of glycerol in aqueous alginate (Ahn et al., 2019), agar (Boral & Bohidar, 2012), and dextran (Antoniou & Alexandridis, 2010) solutions results in polysaccharide conformational swelling (i.e., enhanced solubilisation), whereas higher accumulation of glycerol (>50 vol%) in aqueous carboxymethylcellulose (Jimenez et al., 2022) and dextran (Nalam et al., 2013) solutions has been shown to result in polysaccharide chain collapse (i.e., desolvation). Importantly, this behaviour is not merely confined to water-glycerol mixtures. Swelling and collapse of hyaluronic acid and alginate have been reported in water-organic solvent mixtures containing 1,4-dioxane, tert-butanol, and ethanol (Hermansson et al., 2016; Kutálková et al., 2023). Because polysaccharide folding governs biological function (Liu & Delbianco, 2025) and their conformations critically determine industrially relevant viscoelastic properties (Gericke et al., 2024), it is crucial to understand the mechanism underlying these non-monotonic transitions. The behaviour cannot be reconciled within the standard Flory-type mean-field description because a monotonic collapse of polymeric chains is predicted as the solvent becomes progressively poorer, as is widely reported for synthetic polymers (Baran et al., 1999; Litvinova & Bel'nikevich, 2003). Also, other general frameworks which have the capacity to describe polymer re-entrant behaviour in solutions, such as cosolvency or cononsolvency (Mukherji et al., 2014; Mukherji et al., 2017) are based on both solvents being either good or poor for the polymer, in contrast to water-glycerol which are mixtures of a good and a poorer solvent. Existing explanations have thus relied on explaining the behaviour in terms of specific physicochemical details of polysaccharides and the solvent, such as cooperative hydrogen bonding and hydrophobic interactions (Ahn et al., 2019; Antoniou & Alexandridis, 2010; Boral & Bohidar, 2012; Jimenez et al., 2022; Nalam et al., 2013). Although such interpretations are certainly relevant, a physical description for polysaccharide conformation in binary mixtures of good and poorer solvents remains to be clarified and necessitates for a renewed quest to uncover the underlying mechanism.

Our study investigates the non-monotonic conformational behaviour of polysaccharides in binary mixtures of water and glycerol using a high molecular weight pectin ($\geq 10^7$ g mol^{-1}) extracted from okra (*Abelmoschus esculentus*) fruits as a model polysaccharide. Pectin from okra has high industrial relevance owing to its broad viscoelastic spectrum and high hydration capacity (Mao et al., 2020; Yuan et al., 2018), unique properties that motivated its deliberate and careful selection for this study, enabling direct experimental observation of chain relaxation and solvation. We utilised all-atom simulations and Kirkwood-Buff theory, together with dielectric spectroscopy, neutron scattering, and rheology experiments, to elucidate the mechanism. We hypothesise that the non-monotonic conformational transitions of polysaccharides in water-glycerol mixtures are governed by preferential solvation at the polysaccharide's solvent accessible interface, rather than by mean solvent quality or the average field of the poorer cosolvent. Such non-monotonic transitions would alter chain relaxation and pervaded volume which are expected to map directly to viscoelasticity of polysaccharide solutions. Complementary evidence collectively allowed us to introduce a perspective on solvent entropic penalties and to conclude that the system balances its free energy through a mechanism in which the polymeric chain preserves total water contact by reconfiguring its conformation, with direct consequences for the viscoelastic response. A tentatively unified behaviour is suggestive across complex polysaccharides such as pectin, agar, alginate, carboxymethylcellulose, and dextran, and it appears that this phenomenon is a non-mean-field mechanism with particular relevance to polysaccharides due to the disproportionately high complexity of the polysaccharide-water solvent accessible interface.

2. Materials and methods

2.1. Molecular dynamics simulation

A 24-mer all-atom polysaccharide chain, resembling rhamnogalacturonan-I (RG-I) pectin, was constructed using repeating -[1,2-α-*l*-rhamnose-1,4-*α*-*d*-galacturonic acid] - units in the GLYCAM Carbohydrate Builder (Grant et al., 2026) and topologies were built using Antechamber and Acpype. We have shown earlier (Morris et al., 2010), that RG-I pectin from sugar beet (*Beta vulgaris*) has a persistence length, l_p of ca. 1.4 nm. Accordingly, our 24-mer chain roughly corresponds to three Kuhn segments, i.e., $L/2l_p \approx 3.15$, where the theoretical contour length, $L = Nd\sin\theta/2 \approx 8.80$ nm. Note that θ for C—O—C is 109.5° and d is unit length for Rha-GalA disaccharide ≈ 0.90 nm (Zdunek et al., 2021). The chain length therefore appears adequate for assessing trends in the polysaccharide end-to-end distance, $\overline{R}$, as the infinitely diluted chain shifts from a water (good) to glycerol-enriched (poorer) binary solvent.

Molecular dynamics simulations were performed in GROMACS 2024.1 compiled with CUDA, using the GLYCAM06j-1 parameter set belonging to the GLYCAM06 forcefield family for carbohydrates (Kirschner et al., 2008). No constraints were applied to polysaccharide heavy atoms, glycosidic torsions, or ring conformations during simulation, except for covalent bonds involving hydrogen atoms using the LINCS algorithm. The system was solvated in explicit TIP3P water and AMBER glycerol using a triclinic periodic box. The polysaccharide was centred in the box and with at least 1.2 nm distance from the box edge (box volume, ca. 315 nm^3). 12 Na^+ counterions were used to neutralise the systems. Account of solvent molecules and densities are shown in Supplementary Table S1. Energy minimisation was carried out using the steepest descent algorithm (force ≤100 kJ mol^{-1} nm^{-1}). The C-rescale, V-rescale (modified Berendsen), and the Particle Mesh Ewald method were used for pressure coupling, temperature coupling, and system electrostatics, respectively. Coulomb interactions and van der Waals cutoff were both set to 1 nm, and simulations were run at 298 K, 1 bar of pressure, 4.5×10^{-5} bar^{-1} of compressibility. To account for the glycerol-induced viscosity slowdown of global chain relaxation and

ensure sufficient sampling, we estimated the rotational autocorrelation of the chain's end-to-end vector as, $C(t) = \langle R(0) \bullet R(t) \rangle / \langle R^2 \rangle$ using simulations ranging from 0.10 to 1.20 μs (see Supplementary Fig. S1a, b). The first zero-crossing of $C(t)$ was used as proxy for the longest, Rouse-like relaxation mode ($p = 1$), and are shown in Supplementary Fig. S1c. After identifying the first zero-crossing of $C(t)$, a minimum of $n = 5$ independent replicas were simulated for each system. In these replica simulations, 10 ns of trajectories after the first zero-crossing of $C(t)$, were used to estimate end-to-end distance ($\overline{R}$). These 10 ns sections within each subgroup were concatenated and used for estimation of radial distribution function, $g_{\alpha\beta}(r)$.

2.2. Experimental materials

Glycerol (≥99%), d_5-glycerol (≥98 atom%), phosphorus pentoxide, potassium sulfate, *d*-galacturonic acid, D-fructose, *d*-mannose, *l*-rhamnose, *l*-arabinose, *d*-galactose, D-glucose, *d*-xylose, sulphuric acid, and trifluoroacetic acid were purchased from Sigma-Aldrich, UK and Germany. PELCO® conductive silver paint was purchased from Ted Pella, USA. Milli-Q water (Millipore Corp., USA) was used throughout the experiments (18.2 MΩ·cm at 25 °C). All experiments were carried out at 25 °C, unless otherwise stated.

Pectin polysaccharide was extracted from fresh okra (*Abelmoschus esculentus*) fruits using hot water extraction as described earlier (Yuan et al., 2018), with a few modifications. Briefly, the fruits (moisture content, ca. 88%) were cut into ca. 5 mm-thick slices and heated in water at 55 °C for 90 min (1:10 volume ratio by dry weight basis). The extract was then sieved to remove fruit pulp and centrifuged at 8000*g* for 30 mins to remove any insoluble cellulosic oligomers. The supernatant was dialysed (MWCO 10 kDa or 10^4 g mol^{-1}) against 10 volumes of water for 24 h at 4 °C with three water changes. The viscous liquid was snap frozen at −40 °C using an ethanol bath and then lyophilised. In order to ensure homogeneous mixing and suppress polysaccharide chain scission from excessive shear deformation which is known to occur in polymers with high extensibility (Dinic & Sharma, 2020), the freeze-dried polysaccharide was added to water and then placed on a roller for 24 h for complete dissolution. Note that salts were not added and solution pH was 6.4 after complete pectin dissolution. Following this, glycerol at 0, 20, 40, 60 and 80 vol% was added gravimetrically to the solution and then placed on a roller for another 12 h. Sodium azide was added as an antimicrobial, 0.02% (*w/v*). Detailed characterisation of the extracted polysaccharide was carried out using SEC-MALS and HPAEC-PAD, and results for weight average molar mass, molar mass distribution, monosaccharide composition, total pectic sugars, total RG-I region, and HGA/RG-I ratio are provided in Supplementary Note SN1, SN2. Degree of methyl esterification, predominantly attributed to HGA regions, was ca. 40% and was estimated using infrared spectroscopy on an ATR-FTIR spectrometer (Bruker Optics GmbH, Germany) as described previously (Manrique & Lajolo, 2002), and results are shown in Supplementary Fig. S2.

2.3. Dielectric spectroscopy

Dielectric spectroscopy was performed as a function of field frequency, ν, with a vector network analyser (Anritsu MS4647A), and the setup is described in detail in our earlier study (Ensing et al., 2013). Frequency response in the range of $0.13 \leq \nu$ (GHz) ≤ 70 were probed using open-ended coaxial 1.85 mm probes and SMA connectors. Polysaccharide concentration was 0.2 wt% for all solutions. Pure solvent mixtures (without polysaccharide) were also measured. Sample temperature was controlled using a thermostat silicone oil bath. The reflection coefficient at the coaxial probe and sample interface was calibrated using air, water, and conductive silver paint ($n = 3$).

2.4. Neutron scattering

For neutron scattering, all samples were first dehydrated using phosphorus pentoxide inside a sealed desiccator for 48 h. Dehydrated 80 mg polysaccharides were then rehydrated with water (30 or 70 wt% of polysaccharide), d_5-glycerol was added, sealed in flat aluminium cells using indium, and left to equilibrate for 2 weeks before the experiments. Note that using d_5-glycerol suppressed further H/D exchange.

Quasi-elastic neutron scattering (QENS) scans were performed at 300 K on the Iris time-of-flight inverted geometry spectrometer at the ISIS Neutron and Muon Source in Didcot, United Kingdom (energy transfer range, ± 0.25 meV; resolution, 17.5 μeV; Q, 0.42–1.85 Å^{-1}). Examining the scattering function, S(Q, E) where $E = \hbar\omega$, i.e., the time Fourier transform of the intermediate scattering function, I(Q, t) reveal both static and dynamic correlations among different nuclei (S_{coh}) and the spatiotemporal correlations of identical nuclei (S_{inc}). The incoherent part further contains contributions from vibrational (S_{vib}), translational and/or diffusional (S_{trans}), and rotational or reorientational (S_{rot}) motions as, $S_{inc}(Q,E) = S_{vib}(Q,E) \bigotimes S_{trans}(Q,E) \bigotimes S_{rot}(Q,E) \bigotimes R$, where R is the resolution function (Wang et al., 2024). A single Lorentzian (ensemble-averaged quasi elastic component), Dirac δ-function (mimicking the elastic component), and a linear background was sufficient to fit the $S(Q,E)$ data. Q^2 was limited to $Q < 1.12$ Å^{-1} during fitting to minimise coherent contributions which could dominate the high-Q in deuterated environments, as shown previously by us (Sarter et al., 2024) and others (Arbe et al., 2020). Note that the deuterium structure factor, S(Q) becomes dominant at $Q_{max} \sim 1.95$ Å^{-1}, where $I_{coherant} \sim 6 \bullet I_{incoherant}$ (Arbe et al., 2020). Data were analysed in MANTID.

Elastic fixed window (EFWS) scans were performed on the IN13 thermal neutron backscattering spectrometer at Institut Laue-Langevin in Grenoble, France (EFWS, $\Delta E = 0$ μeV; resolution, 11 μeV; Q, 0.52–4.38 Å^{-1}). Cooling rate was 2 K min^{-1} and data were recorded during the heating phase at 0.34 K min^{-1} in the range of 50–300 K. Temperature-dependant hydrogen mean square displacement, $\langle u^2 \rangle$ was estimated as described previously (Wang et al., 2024), $I_{inc\,elastic}(Q,T)/I_{inc\,elastic}(Q,T_{min}) = exp\left[-\frac{1}{3}Q^2 \left(\langle u \rangle^2 \langle u \rangle^2_{T_{min}} \right) \right]$. Note that the approximation is not valid for larger Q. Readers should also note that Q^2 was limited to $Q < 1.62$ Å^{-1} during fitting, but the coherent scattering does become relevant before our Q^2 maximum. However, the contribution remains limited and does not compromise the validity of the presented results. Data were analysed in LAMP.

Vanadium as reference and empty can measurements were acquired and used for resolution function, data normalisation, and sample correction in both experiments. Transmission for all samples was >90%, ensuring minimal multiple scattering. Mass of all cells was measured after sample preparation, after equilibration, and both before and after the experiments, and ensured no leakage.

2.5. Rheology

The shear rheology response of polysaccharide solutions was characterised on a MCR 301 rotational rheometer with a Peltier temperature control system (Anton Paar, Austria). Measurements were conducted using either (a) sandblasted parallel-plate geometry (plate diameter, 40 mm; gap, 100 μm) fitted with a moisture trap, or (b) concentric cylinder Couette cell geometry for low-viscosity solutions ($\eta_0 \leq 10$ mPa·s). For the data analysis, all appropriate gap-error corrections were applied when the gap errors exceeded the RMS roughness of the plates (Davies & Stokes, 2005). Residual inertia was corrected and any effects of edge fracture, free surface curvature, and secondary flows were aimed to be minimised. Measurements ($n = 3$) were carried out on shear rate ($\dot{\gamma}$) controlled mode of 10^{-1} to 10^3 s^{-1} to measure shear stress, τ, and steady shear viscosity, $\eta(\dot{\gamma}) = \tau/\dot{\gamma}$. The zero-shear viscosity, η_0 was extracted

using the Carreau-Yasuda fitting as, $\eta = \eta_\infty + (\eta_0 - \eta_\infty)\left[1 + (t\dot{\gamma})^a\right]^{\frac{m-1}{a}}$. Normal stress measurements ($n = 3$) were also carried out over the shear rate range of 10^{-1} to 10^4 s^{-1}, utilising the narrow-gap parallel plate method (Davies & Stokes, 2008). Note that once the final gap position was reached, the sample was held until the normal force reached equilibrium (ca. 10 min). Polysaccharide flexibility was described by using the approximations of a finitely extensible nonlinear elastic (FENE)-Fraenkel spring (Pincus et al., 2020). Here, when viscosity is described as a function of shear rate, a $-2/3$ scaling is apparent for springs, while an adequately rigid and rod-like chain shows a $-1/3$ scaling. Considering normal stress profile as, t_{zz} (normal stress) $= -1/2\,\Psi \bullet x^2$ (Rivlin, 1948), where Ψ is the normal stress coefficient and x is the velocity gradient in fluid, the relationship becomes $-1/3$ for springs, conversely $-2/3$ corresponds to rigid and rod-like chains, and was used as such in our data interpretation.

Extensional rheology was carried out on a CaBER-1 extensional rheometer (Thermo Scientific HAAKE, Germany) equipped with an enclosed measuring unit to minimise evaporation and is described in detail in our previous reports (Li et al., 2022; Vaniyan et al., 2025). For all measurements ($n = 5$), we used 76 μL of sample in the parallel geometry (diameter, 6 mm; initial gap and final gap of 3.01 and 9.92 mm, respectively). The strike time was 180 ms with a linear stretch profile to avoid filament oscillations during capillary neck thinning. The initial aspect ratio was 1 and the final aspect ratio was 3.31, corresponding to a step strain deformation rate of 6.63 s^{-1} and Hencky strain of 1.19. Filament thinning data was measured using a laser micrometer and the cut-off for filament thinning was 10 μm in all cases, however some filaments endure for longer periods of time than are represented by the filament thinning data utilised for fitting. Surface tensions and densities were measured using a PAT1 Profile Analysis tensiometer (Sinterface Technologies, Germany) and a DMA 5000 density meter (Anton Paar, Austria), respectively.

3. Results and discussion

Firstly, we will discuss the conformational transitions of an all-atom polysaccharide chain in binary mixtures of water and glycerol. We especially focus on the local occurrence of solvent molecules around the polysaccharide chain, as this sets the stage for understanding the evolution of non-monotonic polysaccharide conformation and its impact on viscoelasticity. Throughout the article, ϕ represents glycerol volume fraction, such that ϕ_0 represents polysaccharide in water, whereas, $\phi_{0.2}$, $\phi_{0.4}$, $\phi_{0.6}$, and $\phi_{0.8}$, correspond to polysaccharide in water-glycerol binary mixtures with nominal glycerol volume fractions of 0.2, 0.4, 0.6, and 0.8, respectively, equivalent to 20 → 80 vol% glycerol.

3.1. Confirming previous observations in polysaccharide conformation

We first demonstrate that a simple 24-mer all-atom chain (Fig. 1a) can reproduce the observable non-monotonic flexible coil → swollen → compact (collapsed) configurations of complex polysaccharides in water-glycerol mixtures. Results are interpreted in terms of the chain's average end-to-end distance, $\overline{R}$ i.e., a measure that reflects conformational swelling and/or collapse (Fig. 1b). Although the chain used in our simulation is stereochemically and topologically nonidentical to the polysaccharides discussed in the introduction, i.e., does not capture the full architectural complexity, including variations in sidechains/branching, counterions, and molecular weight distribution, the overall results demonstrate striking agreement. Here one could observe that in ϕ_0, the median $\overline{R}$ is 6.90 nm and could be considered analogous to the so-called flexible, coil-like conformation of polysaccharides in water. Upon introducing glycerol, we observed the evolution of two prominent conformational states. Initial swelling was followed by the adoption of a more compact (collapsed) configuration. A swelling of the chain is evident for $\phi_{0.2-0.4}$, where median $\overline{R}$ increases to 7.20 and 7.40 nm and approaches the chain's theoretical contour length limit, i.e., 8.82 nm. Upon adding further glycerol in $\phi_{0.6}$, a broad distribution of $\overline{R}$ is apparent. Here, swollen and collapsed conformations coexist. Secondly in $\phi_{0.8}$, the polysaccharide appears to undergo uniform chain collapse, and median $\overline{R}$ decreases to ca. 6 nm. Given that water and glycerol are miscible, one could treat the mixture as an effective single-component solvent. Under this assumption, mean-field theory predicts a monotonic collapse of a polymer chain as the solvent becomes progressively poorer. But results show that chains with constant contour length, firstly undergo ca. 10% swelling in median $\overline{R}$, followed by collapse. Hence the mean-field theory cannot be straightforwardly used to explain the current observations and raises a key question: *what is the local solvent coordination relative to these non-monotonic conformations?* By solvent coordination, we refer to the local occurrence of solvent molecules around the polysaccharide chain, either water or glycerol, which may influence its 'chemical potential'.

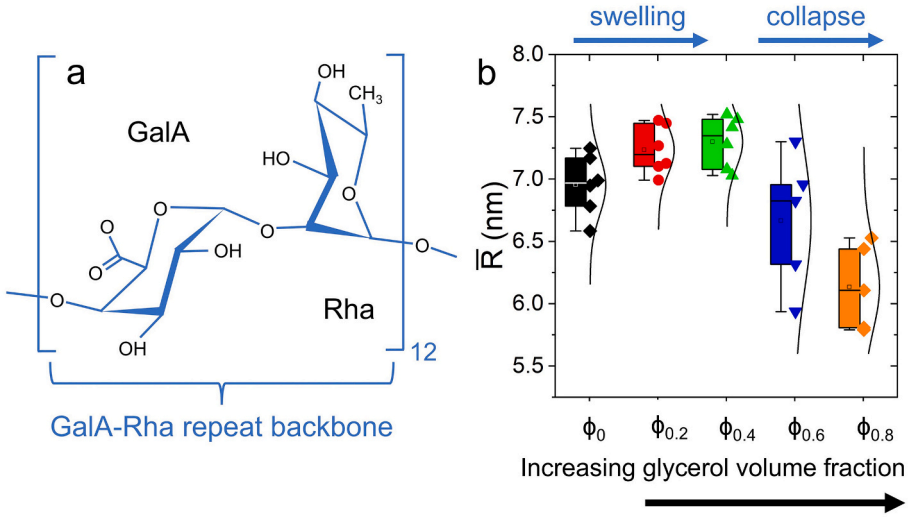

Fig. 1. (a) Illustration shows GalA-Rha repeats in the 24-mer polysaccharide chain used in the all-atom simulations. All hydrogens are not shown explicitly for illustrative purposes. (b) Distribution of average end-to-end distance, $\overline{R}$ of the polysaccharide chain in water-glycerol mixtures, i.e., $\phi_{0\rightarrow0.8}$. ϕ represents glycerol volume fraction. Normal distributions are indicated as black lines, and horizontal lines inside the boxes indicate the median. Samples are indicated as ϕ_0, ■; $\phi_{0.2}$, ●; $\phi_{0.4}$, ▲; $\phi_{0.6}$, ▼; and $\phi_{0.8}$, ♦. Free energy surface and low energy conformations corresponding to $\phi_{0.2\rightarrow0.8}$ are shown in Supplementary Fig. S3.

3.2. Examining the solvent coordination in polysaccharides

To answer this question, we first probed the radial probability distribution from our simulation ensembles, a measure which represents the statistical likelihood of finding either water or glycerol molecules around the solvated polysaccharide chain. Oxygen (O) atoms in polysaccharide, water, and glycerol were used to derive an O—O radial probability distribution, $g_{\alpha\beta}(r)$ between α (polysaccharide, p) and β (water, w or glycerol, g) as, $g_{\alpha\beta}(r) = \frac{\langle \rho_\beta(r) \rangle}{\langle \rho_\beta \rangle_{local}} = \frac{1}{\langle \rho_\beta \rangle_{local}} \bullet \frac{1}{N_\alpha} \sum_{i\epsilon\alpha}^{N_\alpha} \sum_{j\epsilon\beta}^{N_\beta} \frac{\delta(r_{ij}-r)}{4\pi r^2}$. Here $\langle \rho_\beta(r) \rangle$ represents water or glycerol number densities at distance r from the reference atoms in the chain. Results are shown in Fig. 2a, b. One can clearly observe that the first solvation shell, i.e., the innermost layer of solvent molecules around the polysaccharide chain, extends to ca. 0.40 nm (marked by dashed line in Fig. 2a). Interestingly, as the glycerol volume fraction increases in $\phi_{0\rightarrow0.8}$, firstly a decrease in the first solvation shell $g_{pw}(r)$ peak maxima is evident for water in $\phi_{0\rightarrow0.4}$, followed by an increase in $\phi_{0.6\rightarrow0.8}$. Simultaneously, for glycerol, the first solvation shell $g_{pg}(r)$ peak maxima monotonically decrease in $\phi_{0\rightarrow0.8}$. Results for the $g_{pw}(r)$ and $g_{pg}(r)$ peak maxima are shown collectively in Fig. 2c for easier comparison. One can now clearly visualise the progressively changing solvent coordination with a crossover at ca. $\phi_{0.6}$ (illustrated using a dashed blue line in Fig. 2c). This indicates that the local solvent coordination around the polysaccharide chain shifts from being dominated by glycerol to being dominated by water. Note that these molecules in the first solvation shell are still dynamic and in exchange with the unperturbed bulk.

For a more rigorous interpretation, we used the Kirkwood-Buff (KB) solution theory. KB theory is ideal for deriving thermodynamic parameters from radial probability distributions. Here, KB integrals are considered excess volumes, $G^{\infty}_{\alpha\beta} = 4\pi \int_0^{\infty} r^2 \left[g_{\alpha\beta}(r) - 1 \right] dr$ (Smiatek, 2017) and highlight deviations from ideal-solution behaviour due to polysaccharide insertion. Note that our simulation data had finite boundaries, so we applied a finite-size correction as, $G_{\alpha\beta}(r) = 4\pi \int_0^{r} r^2 \left[g_{\alpha\beta}(r) - 1 \right] \left(1 - 3r/2L + r^3/2L^3 \right) dr$ where L denotes a maximum cutoff distance associated with half the simulation box length (Krüger et al., 2013; Milzetti et al., 2018). Fig. 3a, b shows the KB integrals for polysaccharide-water and polysaccharide-glycerol. Here, one can observe that $G_{pw}(r)$ for polysaccharide-water are all negative at large distances, while $G_{pg}(r)$ for polysaccharide-glycerol show a transition from positive to negative values for $\phi_{0.6\rightarrow0.8}$. This indicates that at higher glycerol volume fraction, the cosolvent may be excluded from the polysaccharide's vicinity.

But the polysaccharide-solvent partitioning behaviour cannot be directly explained using KB integrals alone. So, we estimated the finite size corrected preferential binding coefficients for polysaccharide-glycerol as, $\Gamma^{\infty}_{\beta_g\alpha}(r) = \rho_{\beta_g} \left(G^{\infty}_{\beta_g\alpha}(r) - G^{\infty}_{\beta_w\alpha}(r) \right)$ for distances $r \leq L$, where ρ_{β_g} is the number density of species, β_g (Smiatek, 2017). Correspondingly, the preferential hydration coefficient for polysaccharide-water binding was defined as, $\Gamma^{\infty}_{\beta_w\alpha}(r) = -\rho_w/\rho_g \, \Gamma^{\infty}_{\beta_g\alpha}(r)$ (Smiatek, 2017). Results for the preferential binding and hydration coefficients are shown in Fig. 3c, d, respectively. One can now clearly observe high preferential binding coefficients, i.e., $\Gamma_{pg}(r)$ of glycerol molecules to the polysaccharide chain, in terms of positive values at lower glycerol volume fraction, i.e., $\phi_{0.2\rightarrow0.6}$. Conversely, at higher glycerol volume fraction, i.e., $\phi_{0.8}$, the preferential binding coefficient becomes negative and implies glycerol exclusion from the polysaccharide's vicinity. Simultaneously, the preferential hydration coefficients, i.e., $\Gamma_{pw}(r)$ of water molecules become positive at $\phi_{0.8}$, implying hydration of the polysaccharide chain. Both reveal a case of preferential solvation. Here, the relative balance between glycerol and water binding to the polysaccharide chain evolves from preferential binding of glycerol ($\phi_{0.2\rightarrow0.6}$) to preferential hydration of water ($\phi_{0.8}$) as the chain shifts from water to a glycerol-enriched aqueous environment. This behaviour mirrors the corresponding changes in the end-to-end configuration of the polysaccharide seen in Fig. 1b.

3.3. Experimental validation of preferential solvation

To assess the validity of preferential solvation uncovered in our KB analyses, we utilised a high molecular weight pectin ($\geq 10^7$ g mol^{-1}) extracted from okra fruits. We first utilised dielectric spectroscopy which is particularly suitable for dipolar liquids, such as water and glycerol, where the polarisation dynamics stem from the orientational relaxation of dipolar molecules in response to an external, oscillating electric field. Binary mixtures of water-glycerol are already known to show collective (correlated) relaxation in dielectric spectroscopy (Charkhesht et al., 2019). Due to the intrinsic relaxation of these dipoles, polarisation is frequency dependent and exhibits dispersion in the real

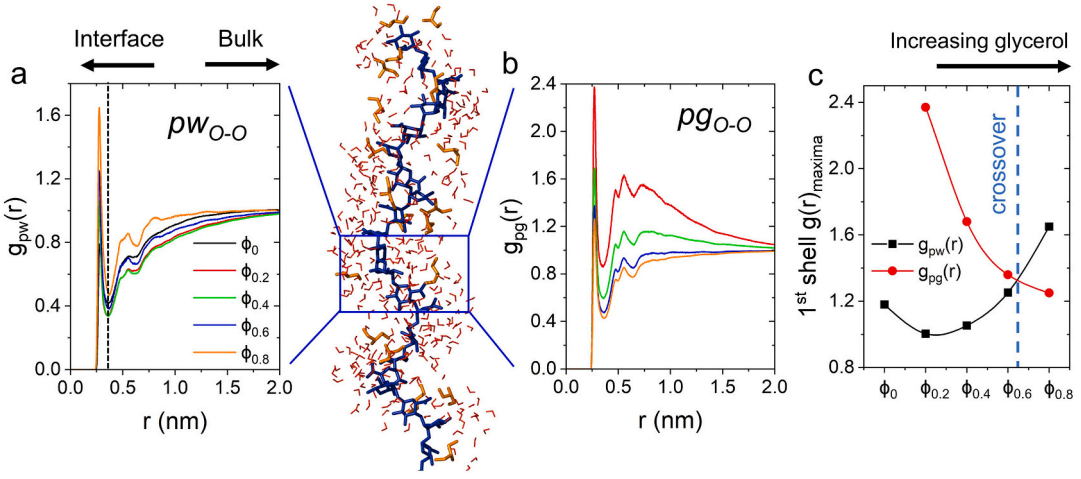

Fig. 2. Oxygen-oxygen (O—O) radial probability distribution, $g_{\alpha\beta}(r)$ of (a) water and (b) glycerol around polysaccharide chain. Black dashed line in (a) is a visual guide to denote the first solvation shell around the polysaccharide. Samples are indicated as ϕ_0 (—); $\phi_{0.2}$ (—); $\phi_{0.4}$ (—); $\phi_{0.6}$ (—); and $\phi_{0.8}$ (—). Illustration depicts distribution of solvents in the first solvation shell around the polysaccharide chain (blue), where water molecules are shown in red and glycerol molecules are shown in orange. (c) First solvation shell maxima for water (■) and glycerol (●) derived from (a) and (b) as a function of solvent composition in $\phi_{0\rightarrow0.8}$. p, polysaccharide; w, water; g, glycerol.

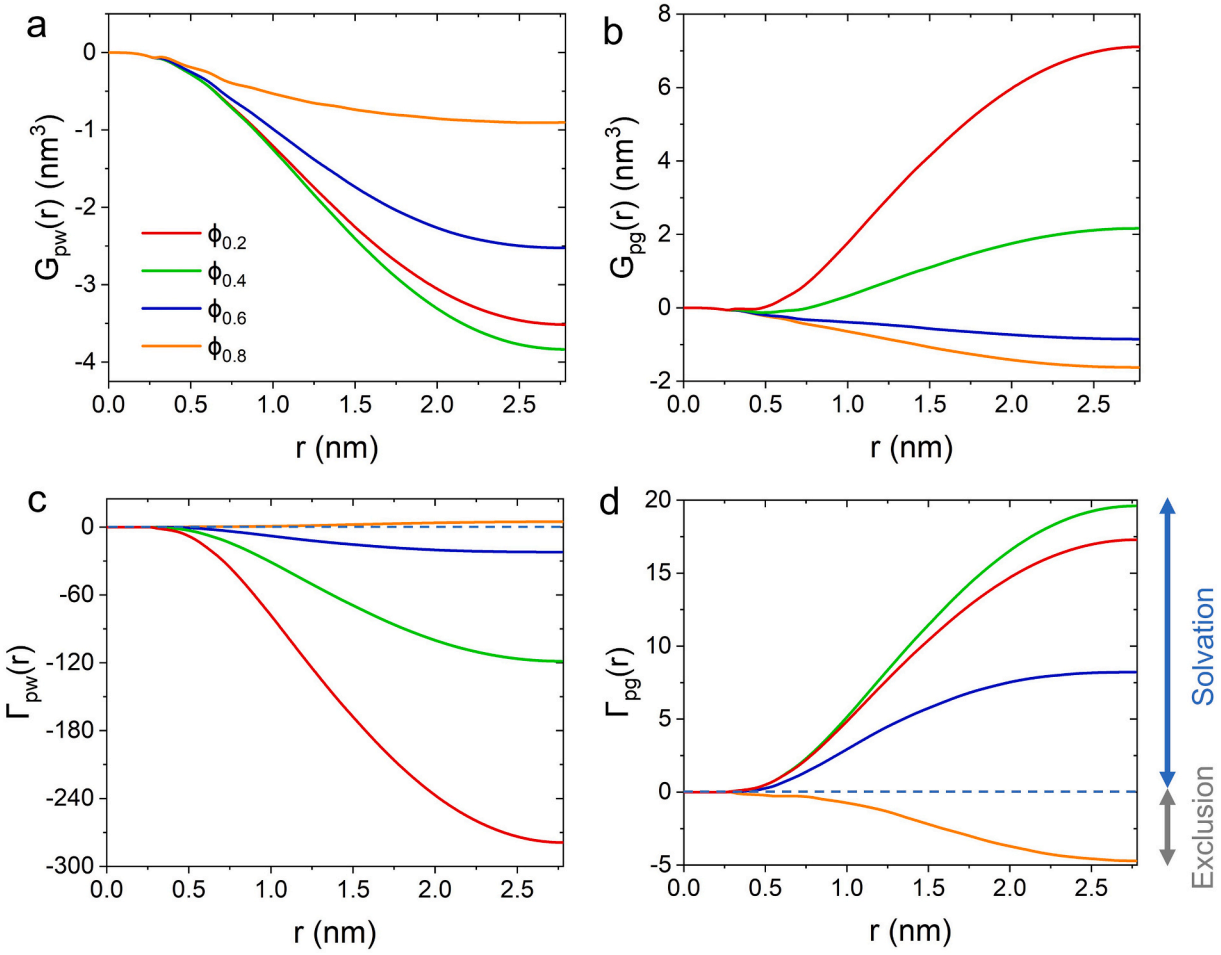

Fig. 3. Kirkwood-Buff integrals, $G_{\alpha\beta}(r)$ for (a) water and (b) glycerol as a function of r distance around the polysaccharide chain in $\phi_{0.2\rightarrow0.8}$. Additional $g_{\alpha\beta}(r)$ and KB integrals for G_{ww}, G_{gg}, and G_{gw} are shown in Supplementary Fig. S4. Preferential hydration and binding coefficients, $\Gamma_{\alpha\beta}(r)$ for (c) water and (d) glycerol as a function of r distance around the polysaccharide chain in $\phi_{0.2\rightarrow0.8}$. Dashed blue lines are a visual guide to demarcate the preference for solvation versus exclusion of solvent from the polysaccharide. Samples are indicated as $\phi_{0.2}$ (—); $\phi_{0.4}$ (—); $\phi_{0.6}$ (—); and $\phi_{0.8}$ (—). p, polysaccharide; w, water; g, glycerol.

part, i.e., $\varepsilon'(\nu)$ and peaks in the imaginary part, i.e., $\varepsilon''(\nu)$. Any deviation from the pure solvent behaviour, i.e., preferential solvation occurring due to polysaccharide insertion, can therefore be readily captured from the relaxation response.

We express the measured polarisation as complex permittivity, $\widehat{\varepsilon}(\nu) = \varepsilon'(\nu) - i\varepsilon''(\nu) + \kappa/2\pi i\nu\varepsilon_0$, where $\varepsilon'(\nu)$ represents dielectric

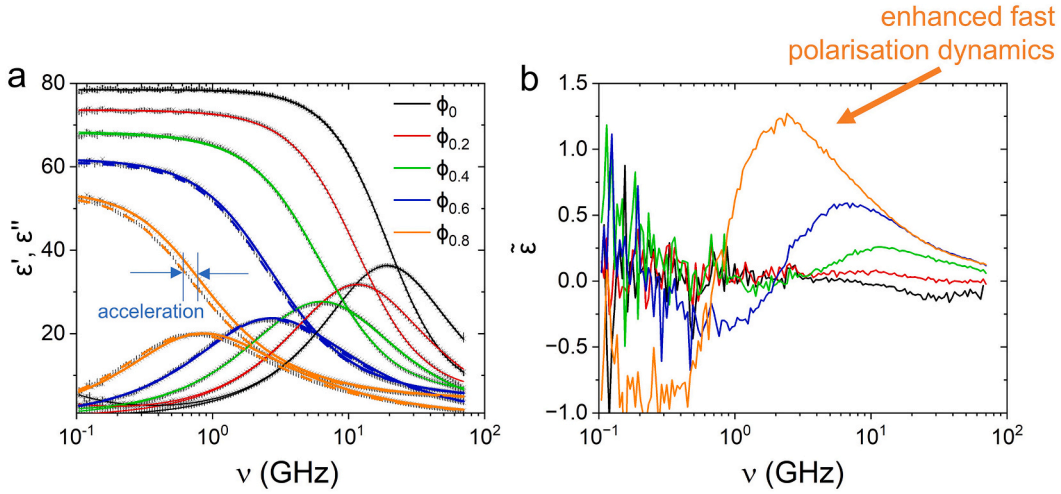

Fig. 4. (a) Complex permittivity of polysaccharide solutions (×) and the water-glycerol solvent (|) as a function of frequency, ν. Fitted Havriliak-Negami relaxation models are indicated as solid lines (polysaccharide solutions) and as dashed lines (solvents, without polysaccharide). Denoted acceleration is a visual guide. (b) Differential loss spectra. Polysaccharide (pectin from okra) concentration was 0.2 wt%. Samples are indicated as ϕ_0 (—); $\phi_{0.2}$ (—); $\phi_{0.4}$ (—); $\phi_{0.6}$ (—); and $\phi_{0.8}$ (—).

permittivity, $\varepsilon''(\nu)$ represents the dielectric loss, and $\kappa/2\pi i\nu\varepsilon_0$ was used to correct for minor contributions of conductivity. To describe the results in terms of relaxation time, τ, we fit the $\varepsilon'(\nu)$ and $\varepsilon''(\nu)$ simultaneously using a single Havriliak-Negami relaxation mode and a conductivity term as, $\widehat{\varepsilon}(\nu) = \Delta\varepsilon/(1+(i2\pi\nu\tau)^{\alpha})^{\beta} - i\left(\kappa/2\pi\nu\varepsilon_0\right) + \varepsilon_\infty$. Results are shown in Fig. 4a and Table 1. For pure water, the predominant relaxation is centred at 19.3 GHz, corresponding to a relaxation time, $\tau = 8.26$ ps. Upon adding glycerol to water, the dielectric response shifts progressively to lower frequencies, indicating a slowdown of the collective (correlated) relaxation dynamics, and agrees with previous literature (Charkhesht et al., 2019). Remarkably, upon insertion of polysaccharide into the water-glycerol mixtures, we observe a moderate, yet significant acceleration of the overall polarisation dynamics at high glycerol volume fraction, i.e., in $\phi_{0.6}$ and $\phi_{0.8}$. This is evident from the shift in the dispersion to higher frequencies (see visual guide indicating the acceleration in $\phi_{0.8}$, Fig. 4a). For further clarity, we have shown the differential loss spectra, $\widetilde{\varepsilon}(\nu) = \widehat{\varepsilon}(\nu)_{solution} - \widehat{\varepsilon}(\nu)_{solvent}$ corrected for κ (conductivity term) derived from the Havriliak-Negami fitting, in Fig. 4b. Here, one can clearly observe the negative contributions at low frequencies (i.e., reduced slow relaxation dynamics) and positive contributions at higher frequencies (i.e., enhanced fast polarisation dynamics). The accelerated dynamics are ca. 10 and 45 ps for $\phi_{0.6}$ and $\phi_{0.8}$ solutions, respectively (cp. τ in Table 1 for solutions versus solvent). It is unlikely that the acceleration is a polysaccharide contribution, as we have shown earlier using alginate, that the overall polarisation dynamics of the solvent is rather insensitive to polysaccharide concentration (Mazur et al., 2014). Also, notice that acceleration was not observed in our $\phi_{0\rightarrow0.4}$ data. Results for $\phi_{0.6}$ and $\phi_{0.8}$ therefore indicate towards a decrease of collective (correlated) relaxation in water-glycerol mixtures and concur with the observations from KB analyses. Preferential hydration of the polysaccharide, alongside the glycerol exclusion, likely reduces the water-glycerol collective (correlated) relaxation. This reduced correlation is observed as acceleration of dynamics in our study, consistent with previous reports linking reduced correlation to acceleration (Rinne et al., 2014). Note, polysaccharide concentration was 0.2 wt% in our measurements. Reducing the concentration by half, i.e., 0.1 wt%, lowers the magnitude of acceleration in $\phi_{0.6}$ and $\phi_{0.8}$ relative to solvent mixtures (data not shown). This indicates that the polysaccharide actively biases the solvent's collective dynamics in $\phi_{0.6}$ and $\phi_{0.8}$.

For a complementary, but more direct, observation of the nanoscale water dynamics, we utilised quasi-elastic neutron scattering (QENS) with careful control of polysaccharide hydration. This was our second, more local validation, focused on solvation shell water. In QENS, relaxation and/or diffusional processes are observed as broadening of the quasi-elastic linewidth in the energy transfer function (Wang et al., 2024). We hypothesised that, if dielectric spectroscopy correctly described the reduced correlation in $\phi_{0.8}$, a preferentially solvated layer of water would exhibit a correlation time akin to the observations for nanoconfined water (ca. 30 ps) (Swenson et al., 2000), which is markedly different when compared to pure bulk water (ca. 1–2 ps). Albeit, in the absence of preferential solvation, a faster correlation time for water akin to observations in 80 vol% aqueous glycerol (ca. 10–15 ps) (Nakagawa & Oyama, 2019) was likely. For careful control of hydration, we first quantified the localised (non-freezable) water content in the polysaccharide, which was 0.97 g g^{-1} polysaccharide; considerably higher than proteins and glycoproteins, e.g., 0.34 g g^{-1} for lysozyme (Miyazaki et al., 2000) and 0.51 g g^{-1} for mucins (Znamenskaya et al., 2012). Note that non-freezable water does not represent water trapped in the interstices within biomacromolecule structures, which can be much higher for heavily glycosylated systems (Harding et al., 1983). Within this localised water population, bound water < 50 wt% < intermediate water (see Supplementary Note SN3 for calorimetry details). Both populations are dynamically coupled to the polysaccharide and represent water at, or slightly above, monolayer coverage. Investigating a system with intermediate water also enables water interactions not only with the polysaccharide chain but also among neighbouring water molecules, in principle, mimicking the three-dimensional (correlated) network in solutions (Russo & Teixeira, 2015).

Preliminary QENS scans were carried out with 30 and 70 wt% hydrated samples to probe both the bound and intermediate water regimes. A dry sample was also examined. Quasi-elastic broadening on the instrumental timescale was observed only at 70 wt% hydration. In contrast, the dry or 30 wt% hydrated sample did not show appreciable linewidth broadening (Supplementary Fig. S5). Results indicate that the signal predominantly arises from the intermediate water population and was apt for hypothesis testing. Guided by this, linewidth broadening for the 70 wt% hydrated sample, both in the absence and presence of d_5-glycerol, was examined and results are shown in Fig. 5a. Observations of FWHM suggest Q^2-independent behaviour, which we interpret as localised (e.g., rotational), non-translational dynamics. Weighted arithmetic means of the FWHM, i.e., Γ_{eff}, gave us a characteristic correlation time, $\tau = 2\hbar/\Gamma_{eff}(Q)$ of ca. 43.44 ± 1.84 ps without d_5-glycerol and 46.85 ± 1.58 ps with d_5-glycerol. Both observations are close to the dynamics of nanoconfined water. Taken together, the results demonstrate that water remains localised around the polysaccharide chain undergoing rotational dynamics. Importantly, glycerol does not desorb this population, further confirming the reduced water-glycerol correlation due to preferential solvation, which led to the acceleration of dynamics observed in dielectric experiments as we had tacitly assumed. Note that we did not examine $\phi_{0.4}$ because no specific spectroscopic features were observed in dielectric spectroscopy. Moreover, preferential solvation of polysaccharide with glycerol and the corresponding exclusion of water into the bulk was expected to result in a water correlation time closer to that of 40 vol% aqueous glycerol, ca. 5–6 ps (Nakagawa & Oyama, 2019), which lies outside the timescale of the spectrometer used in this study.

Table 1
Dielectric relaxation parameters derived from the Havriliak-Negami fitting.

	Polysaccharide solutions				Water-glycerol solvents			
	τ (ps)	α	β	κ (S m^{-1})	τ (ps)	α	β	κ (S m^{-1})
ϕ_0	8.29 ± 0.01	0.99	1	0.02	8.26 ± 0.01	0.99	1	ND
$\phi_{0.2}$	13.71 ± 0.02	0.96	1	0.01	13.68 ± 0.02	0.96	1	ND
$\phi_{0.4}$	25.03 ± 0.06	0.92	1	ND	25.23 ± 0.07	0.92	1	ND
$\phi_{0.6}$	67.42 ± 1.47	0.92	0.84	ND	74.65 ± 1.81	0.94	0.80	ND
$\phi_{0.8}$	248.03 ± 1.31	0.95	0.71	ND	293.61 ± 1.39	0.97	0.68	ND

τ is the relaxation reorientation time. α and β represent symmetric and asymmetric width of the time-constant distribution, and κ is the conductivity term. For $\phi_{0-0.4}$, where β = 1, the mode is equivalent to Cole-Cole relaxation. ND, not detected. ps, picosecond; S m^{-1}, Siemens per meter. Polysaccharide (pectin from okra) concentration was 0.2 wt%. $n = 3$.

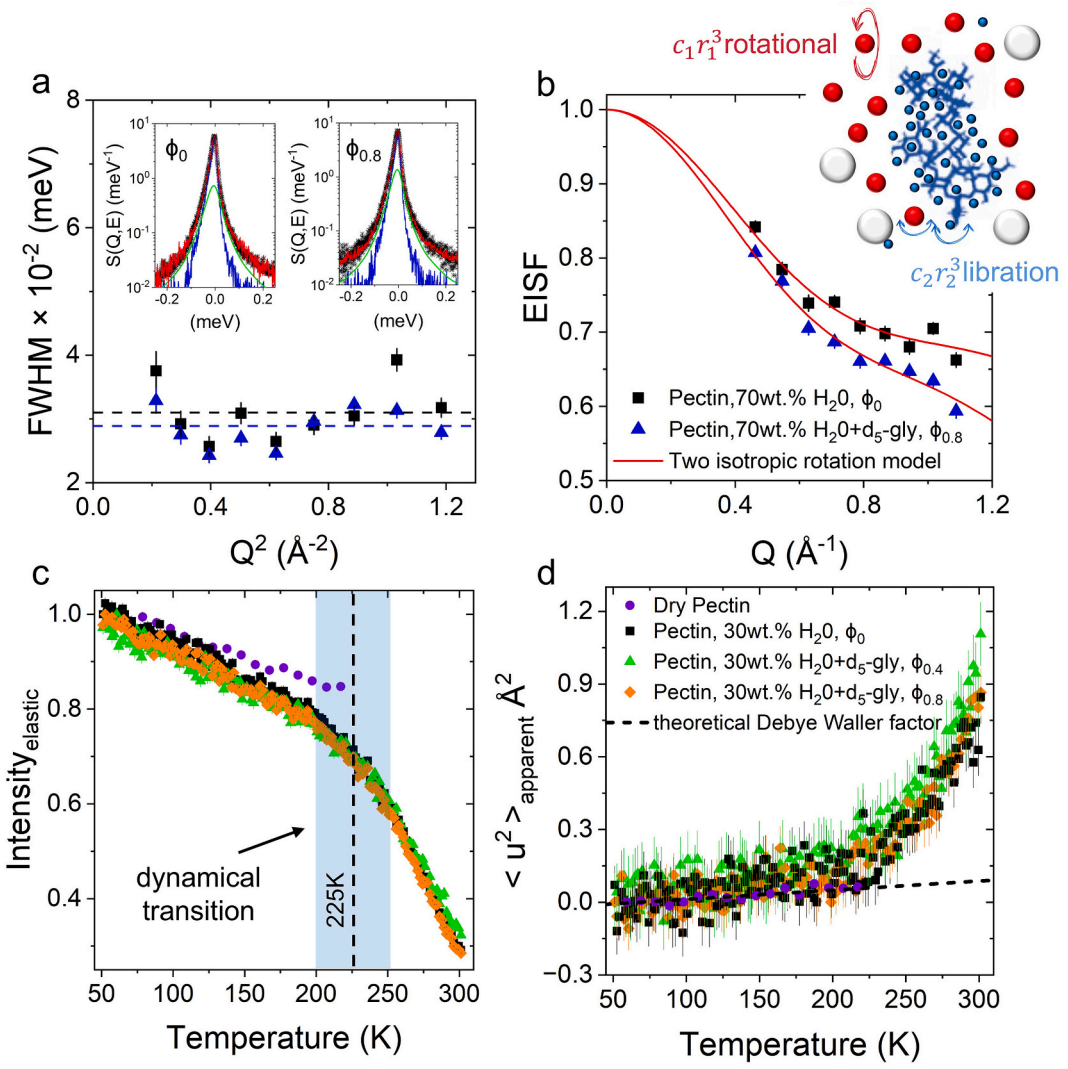

Fig. 5. (a) Linewidth full width half maximum (FWHM, Γ_{eff}) as a function of Q^2 measured using quasi-elastic neutron scattering (QENS, energy transfer, ±0.25 meV) at 300 K. Dashed black and blue lines are weighted arithmetic means. Insets show S(Q, E) as a function of energy transfer (meV), where data (∗), overall fit (—), Dirac δ-function (—), and Lorentzian (—) are shown; left panel (without d_5-glycerol) and right panel (with d_5-glycerol) at Q, 1.08 $Å^{-1}$. (b) Elastic incoherent structure factor (EISF) as a function of Q. Inset shows illustration of dynamic contributions arising from intermediate water (in red), and bound water and polysaccharide (in blue). d_5-glycerol (suppressed incoherent signal) is depicted in grey. (c) Elastic fixed window scans (EFWS, $\Delta E = 0$ μeV) as a function of temperature. The intensity scale is normalised to data at 50 K. Blue shading visually indicates the region corresponding to the onset of dynamical transitions, and black dashed line denotes the median. (d) Temperature-dependent mean-square displacement, $\langle u^2 \rangle$ derived from EFWS. Black dashed line indicates extrapolation of $T \leq 100$ K for dry polysaccharide (theoretical Debye-Waller factor). Legends are shown only in (b) and (d): those in (b) are identical to (a), and in (d) are identical to (c).

3.4. Entropy of preferential solvation

QENS data corresponding to $\phi_{0.8}$ were further modelled to quantify the associated entropy change in the intermediate water using the elastic incoherent structure factor (EISF) termed as $A_0(Q)$, which is a measure that reflects the ratio of elastic to total incoherent (elastic and quasi-elastic) scattering intensity. EISF are shown in Fig. 5b and one can observe that the decrease of A_0(Q) is more pronounced in the presence of glycerol. We used the combination of two isotropic rotations to describe the data as, $A_0(Q) = \sum_{n=1}^{2} c_n j_0^2(Qr_n)$ (Hernandez-Tamargo et al., 2021), where r_n (comprising, r_1 and r_2) are the radii of localised rotations within a confined domain, c_n (comprising, c_1 and c_2) are the fractional contribution of each motion to $A_0(Q)$, and $j_0 = \sin(Qr)/_{Qr}$ is the spherical Bessel function. Note that the data could not be described by the single isotropic rotation or rotation inside a sphere (Volino-Dianoux) model. From the two isotropic rotations model, the extracted radii r_1 and r_2 were, 3.47 ± 0.44 and 0.51 ± 0.22 Å for hydrated polysaccharide, and 3.77 ± 0.31 and 0.75 ± 0.09 Å for hydrated polysaccharide with d_5-glycerol. Corresponding contributions, c_1 were 0.25 ± 0.05 and 0.24 ± 0.03, respectively (note, $c_2 = 1 - c_1$). The values of r_1 are comparable to the size of a water molecule (ca. 3 Å), suggesting that the contribution arises from localised rotational motion of intermediate water molecules, contributing ca. 25% to the overall dynamics (consistently, 20% of total water in the polysaccharide was intermediate). Here r_2 likely corresponds to highly localised motions (e.g., libration motions in intermediate or bound water and polysaccharide) and is illustrated in Fig. 5b. The associated entropy change was estimated as described earlier (Fitter, 2003), using the r_1 parameters as, $\Delta S_{hydr} = 3Rln\frac{r_{\text{hydrated polysaccharide with glycerol}}}{r_{\text{hydrated polysaccharide}}}$ revealing a modest entropy increase of ca. 2.14 ± 0.91 J K^{-1} mol^{-1} in the intermediate water population ($\approx 0.27K_BT$). Note that $\Delta S_{hydr} = \Delta S - \Delta S_{conf}$, where ΔS_{conf} is the conformational entropy of the polysaccharide.

Further experiments were carried out in the elastic fixed window scanning (EFWS) mode. In this mode, a transition from the elastic in-

tensity indicates the activation of relaxation and/or diffusional processes. Note that in these experiments, we focussed on the polysaccharide (segmental) dynamics, thus hydration was maintained at 30 wt% to suppress contributions from intermediate water. Normalised EFWS straightforwardly revealed the onset of a prominent relaxation centred at ca. 225 K in hydrated samples (Fig. 5c). Given the probed Q range of 0.52–4.38 $Å^{-1}$, the results include large- to small-scale motions, and 225 K is likely the glass transition temperature of hydrated pectin and reflects the onset of solvent-coupled polymer segmental dynamics (see additional information in Supplementary Note SN4). Similar transitions near 220–230 K have been reported in other macromolecules, including proteins and DNA, and are attributed to thermodynamic and structural changes in hydration water (Kumar et al., 2006). Following the dynamical transition, mean square displacement, $\langle u^2 \rangle$ for the hydrated sample increased to 0.77 ± 0.11 $Å^2$ at 300 K. In the presence of d_5-glycerol, the corresponding values increased to 1.11 ± 0.13 for $\phi_{0.4}$ but only marginally to 0.86 ± 0.09 $Å^2$ for $\phi_{0.8}$ (Fig. 5d). Results indicate ca. 40% higher segmental dynamics in $\phi_{0.4}$, compared to ϕ_0 and $\phi_{0.8}$ at 300 K. The associated entropy change was estimated as described earlier (Stadler et al., 2015) using the $\langle u^2 \rangle$ parameters as, $\Delta S_{conf} = 3Rln\sqrt{\frac{\langle u^2 \rangle_{\text{hydrated polysaccharide with glycerol}}}{\langle u^2 \rangle_{\text{hydrated polysaccharide}}}}$ revealing a conformational entropy increase of ca. 4.46 ± 0.23 J K^{-1} mol^{-1} (≈ 0.57K_BT) in $\phi_{0.4}$. No significant increase in conformational entropy was observed for $\phi_{0.8}$.

Taken together, our results indicate that at lower glycerol volume fraction, polysaccharide swelling is accompanied by an increase in conformational (segmental) entropy. In contrast, at higher glycerol volume fraction, polysaccharide collapse is associated with a modest increase in the entropy of hydration water, while no appreciable increase in conformational entropy is observed. We would like to note that accurate entropy estimation is challenging and may be affected by correlations outside the instrumental timescales. However, our results from both QENS and EFWS appear reasonable considering that similar results have been observed in myoglobins where ΔS_{hydr} in the folded (collapsed) state was higher compared to the unfolded (swollen) state (Stadler et al., 2015). Similarly, increased ΔS_{conf} was observed in the unfolded structure of bacterial α-amylase (Fitter, 2003).

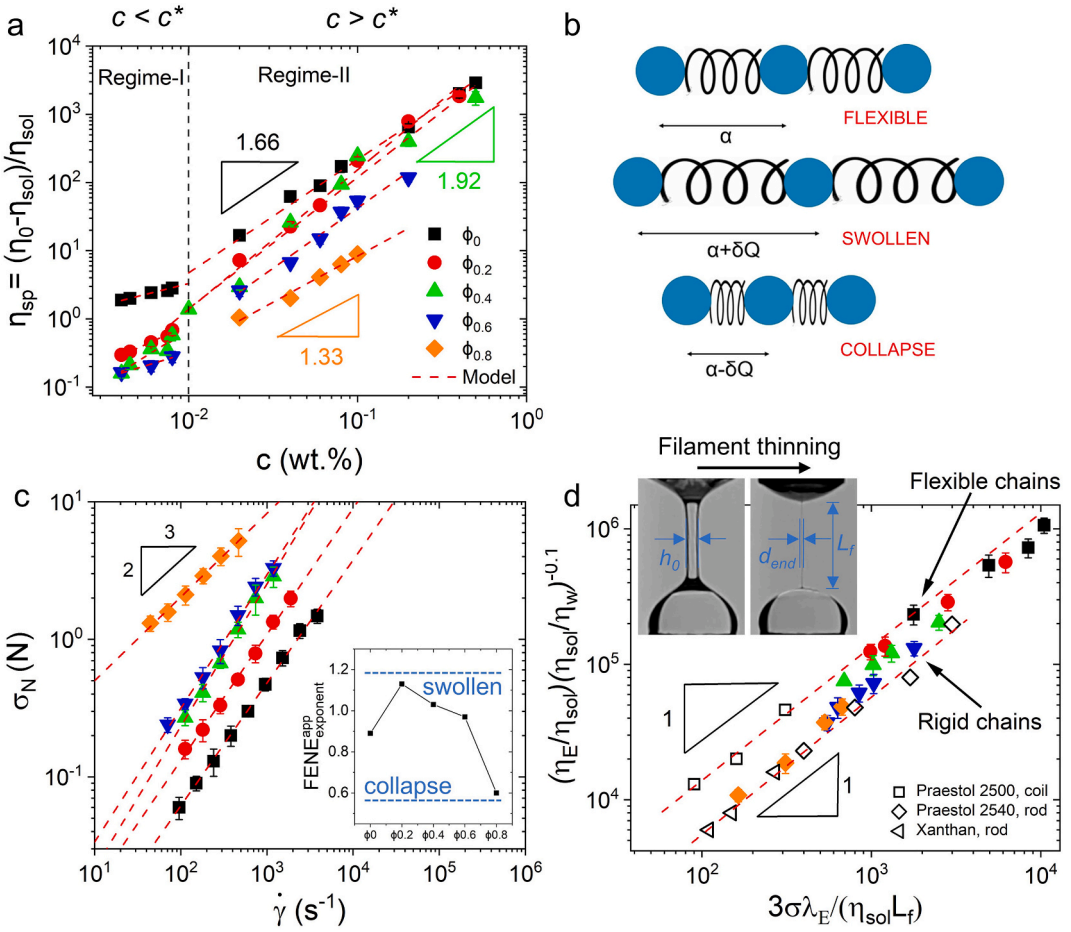

Fig. 6. (a) Specific viscosity, η_{sp} as a function of the polysaccharide concentration, c for $\phi_{0\rightarrow0.8}$. Red dashed lines show power law fits. Black dashed line is a visual guide to demarcate the boundaries of Regime-I and -II. Shear viscosity (η) and shear stress (τ) as a function of shear rate ($\dot{\gamma}$) for $\phi_{0\rightarrow0.8}$ are shown in Supplementary Fig. S6. (b) Illustration depicts the flexible, swollen, and collapsed interpretations in the FENE-Fraenkel spring approximation; α is the relaxed spring length and δQ is the change in spring length. (c) FENE description of normal stress (σ_N) as a function of shear rate ($\dot{\gamma}$) in c, 0.5 wt% polysaccharide solutions. Dashed red lines show power law fits. Inset shows $FENE^{app}_{exponent}$ as a function of $\phi_{0\rightarrow0.8}$. Raw data for normal stress are shown in Supplementary Fig. S6.1f. (d) Dimensionless η_E as a function of dimensionless λ_E alongside concentration-dependent variation in $\phi_{0\rightarrow0.8}$ during filament thinning. Here, η_{sol}, η_w, σ, and L_f are shear viscosity of solvent, shear viscosity of water, surface tension of solution, and filament length, respectively. Dashed red lines correspond to flexible and rigid polysaccharides. Data for praestol (2500 and 2540) and xanthan solutions are renditions of the original data by others and are detailed in the manuscript. Inset illustrates the initial exponential thinning followed by a linear cylindrical thinning in the late stage for 0.2 wt% $\phi_{0.4}$ solution during capillary breakup extensional rheology, where h_0 is initial filament diameter at the onset of elastocapillary regime, d_{end} is filament diameter in the terminal regime, and L_f is filament length. Polysaccharide concentration ranges were ϕ_0, 0.2–0.8 wt%; $\phi_{0.2}$, 0.08–0.4 wt%; $\phi_{0.4}$, 0.06–0.2 wt%; $\phi_{0.6}$, 0.04–0.2 wt%; and $\phi_{0.8}$, 0.02–0.08 wt%. Raw data for filament thinning, surface tensions, and density are shown in Supplementary Note SN6 and Fig. S7. In (a), (c), and (d), samples are indicated as ϕ_0, ■; $\phi_{0.2}$, ●; $\phi_{0.4}$, ▲; $\phi_{0.6}$, ▼; and $\phi_{0.8}$, ♦.

3.5. Viscoelasticity of polysaccharide solutions

A key consequence of preferential solvation and the emergence of non-monotonic conformational transitions is its impact on viscoelasticity. We quantified the apparent force constant as, $\langle k \rangle^{app} = \frac{3K_B}{\langle u^2 \rangle_{dT}}$ in the anharmonic regime above the dynamical transition from EFWS (Zaccai, 2000). For ϕ_0, $\phi_{0.4}$, and $\phi_{0.8}$, $\langle u^2 \rangle_{dT}$ in the linear regime between 275 and 300 K were $8.18 \pm 2.25 \times 10^{-3}$, $16.04 \pm 2.27 \times 10^{-3}$, and $12.88 \pm 1.23 \times 10^{-3}$ Å^2 K^{-1}, respectively. Respective $\langle k \rangle^{app}$ were 50.60 ± 13.90, 25.80 ± 3.70, and 32.20 ± 3.10 pN Å^{-1}. Although our EFWS experiments utilised partially hydrated polysaccharides, compared to ϕ_0, $\phi_{0.4}$ demonstrated ca. 50% lower segmental stiffness (i.e., enhanced flexibility), whereas $\phi_{0.8}$ partially recovers the stiffness within the probed experimental conditions and instrumental timescale.

To contextualise the observations within the framework of polymer solution theory in dilute or semi-dilute solutions, we first determined the polysaccharide's overlap concentration, c^*, using shear rheology. Specific viscosity, $\eta_{sp} = (\eta_0 - \eta_s)/\eta_s$ was measured to establish the limits of dilute to semi-dilute regimes in the solutions (η_0 is the zero-shear viscosity and η_s is the solvent viscosity). c^* for ϕ_0 was ca. ≥ 0.01 wt%. Note that c^* could not be clearly defined for $\phi_{0.2\to0.8}$. Based on c^* for ϕ_0, a suggestive two regime demarcation as a function of polysaccharide concentration is presented in Fig. 6a (Regime-I $< c^* <$ Regime-II). The scaling in Regime-I implies $\eta_{sp} \propto c^{1/2}$, $c^{3/2}$, $c^{3/2}$, and $c^{1/2}$, for $\phi_{0\to0.6}$, respectively (note, scaling for $\phi_{0.8}$ was not detected in Regime-I). The scaling in Regime-II broadly implies $\eta_{sp} \propto c^{3/2}$ for $\phi_{0\to0.8}$. In Regime-I and -II, Fuoss law describes the $c^{1/2}$ scaling as characteristic behaviour for semi-dilute, unentangled solutions of polymer chains and for semi-dilute unentangled combs, whereas $c^{3/2}$ scaling matches the scaling theory prediction for polymer combs with entangled backbones and unentangled side chains (Jimenez et al., 2020). Note, at $c >$ c*, the polysaccharide chains appear to overlap extensively, leading to a regime where viscosity increases strongly with polysaccharide concentration. While this Fuoss regime may be described as 'semi-dilute entangled', in this work we use the term 'semi-dilute' to avoid confusion.

Our primary focus was the semi-dilute regime ($c > c^*$). We described the polysaccharide flexibility using the scaling of normal stresses, σ_N at high shear rate, $\dot{\gamma}$ by using the approximations of a FENE-Fraenkel spring (Pincus et al., 2020). Finite extensibility results from the saturation of the stress caused by excessively stretched and orientated polymers, where $-1/3$ power law scaling corresponds to springs, and $-2/3$ scaling corresponds to rigid and rod-like chains (see details in Section 2.5). A natural way to compare these 'springs' and 'rods' with swollen and collapsed chain conformations is illustrated in Fig. 6b. Results shown in Fig. 6c correspond closely to the trends of FENE-Fraenkel dumbbell scaling behaviour with exponents of 0.89, 1.13, 1.03, 0.97 and 0.55 for $\phi_{0\to0.8}$, respectively, and appear consistent with swollen and collapsed configurations (Fig. 6c, inset). Note that the terms swollen or collapsed are approximations when applied to semi-flexible, branched, and compositionally heterogeneous polysaccharides. Our FENE trends are consistent with dilute regime ($c \ll c^*$) analysis (Supplementary Note SN5) but should be considered as a first-order approximation of the system's behaviour under shear.

Additional extensional viscosity measurements were employed. In such experiments, a sufficiently thin liquid filament bridge is formed where surface tension drives filament thinning and generates uniaxial extensional flow (illustrated in Fig. 6d, inset). Apparent relaxation time, λ_E was estimated from the elastocapillary regime as, $d = d_0 e^{-t/3\lambda_E}$ and terminal extensional viscosity, η_E was estimated at longer t, as $d = d_0 - \sigma/\eta_E\, t$, where σ is the surface tension (Stelter et al., 2002). Further discussions and results are in Supplementary Note SN6. In order to enable a comparison across solvent viscosities and polysaccharide concentrations, we report λ_E and η_E as dimensionless reduced variables in Fig. 6d, using a normalisation procedure described earlier (Stelter et al., 2002). Fig. 6d shows two reduced η_{E/λ_E} dependencies, both with ca. $\eta_E \propto \lambda_E{}^1$ scaling. Here, $\phi_{0\to0.4}$ tends to follow a primary dependency, while $\phi_{0.6\to0.8}$ follows a secondary dependency. Stelter and coworkers (Stelter et al., 2002), describe the primary dependencies towards flexible polymer behaviour, while the secondary dependency is considered to arise from more compact, rigid-like polymer conformation and/or a weaker stretching contribution. Although comparing our data with flexible praestol 2500, rigid praestol 2540, and xanthan rods reported earlier (Stelter et al., 2002) shows consistency with the description (Fig. 6d), finite extensibility, molecular weight distribution, and the apparent nature of λ_E may influence the observed scaling. Results nevertheless indicate a translation of conformation into viscoelastic responses, where extensional viscosity appears to emerge from the contribution of swollen coils or compact (collapsed) polysaccharide conformations to the bulk stress. Note that a chain of length, $2L$, will contribute equally to bulk stress as that by a rigid sphere of radius L in pure strain state (Batchelor, 1971), therefore, as L gets smaller, the contribution to bulk stress reduces.

3.6. Unified perspective and mechanism

Summarising our results on pectin and those of other reported polysaccharides, including agar (Boral & Bohidar, 2012), alginate (Ahn et al., 2019), carboxymethylcellulose (Jimenez et al., 2022), and dextran (Antoniou & Alexandridis, 2010) in water-glycerol mixtures, expressed in units of R_g^{app}, leads to a tentatively unified perspective. Note that for pectin and carboxymethylcellulose, $R_h^{app} = \left(3M[\eta]/10\pi N_A\right)^{1/3}$ (García de la Torre & Hernández-Cifre, 2025). All experimental data, except alginate which was originally reported as $\left\langle R_g^2 \right\rangle_z^{1/2}$, are translated to theoretical R_g^{app} for uniformity, using a Gaussian limit of 1.50 (Haydukivska et al., 2020) when glycerol <50 vol%, and a uniform hard sphere limit of $\sqrt{3/5}$ (Zhang & Wu, 2001) when glycerol >50 vol%. From our simulations of the simple all-atom chain, we additionally utilise the values for Γ_{pg} at large distances away from a polysaccharide chain to estimate, $\Delta\mu_p^{tr} = -RT\Gamma_{pg}$ (Baynes & Trout, 2003), where $\Delta\mu_p^{tr}$ is the transfer free energy required to insert a polysaccharide chain in the glycerol-enriched solutions. Results are plotted alongside R_g^{app} in Fig. 7. A characteristic picture of polysaccharide swelling and collapse emerges from this comparative analysis. A lower transfer free energy corresponds to higher polymer solubility; hence, one would typically expect the polysaccharide transfer free energy to increase as solvent quality deteriorates. But our observations of a decreasing transfer free energy in $\phi_{0.2-0.4}$ mirrors the conformational swelling across the complex polysaccharides, a behaviour at odds with the predictions of the mean-field theory. In other words, polysaccharide solubility is not determined solely by the average field of the poorer cosolvent. Qualitatively, the observed non-monotonic behaviour is irrespective of specific polysaccharide chemistry, suggesting that a broad range of polysaccharides may show similar behaviour, as long as the preferential solvation picture is consistent.

Considering our preferential solvation and $\Delta\mu_p^{tr}$ arguments in relation to polysaccharide conformation, let us now review an infinitely dilute polysaccharide chain (solute, p) in a binary solvent of water, w and glycerol, g, at fixed temperature, T and pressure, P. Within the fluctuation solution theory, transfer free energy of solute, μ_p^{tr} would depend on the glycerol chemical potential, μ_g as, $\left(\partial\mu_p^{tr}/\partial\mu_g\right)_{T,P,N_w} = -\langle \delta N_P \delta N_g \rangle / \langle N_p \rangle$ where the covariance $\langle \delta N_P \delta N_g \rangle$ denotes the polysaccharide and glycerol number correlation. Now, performing a statistical variable transformation to connect fluctuation solution theory to

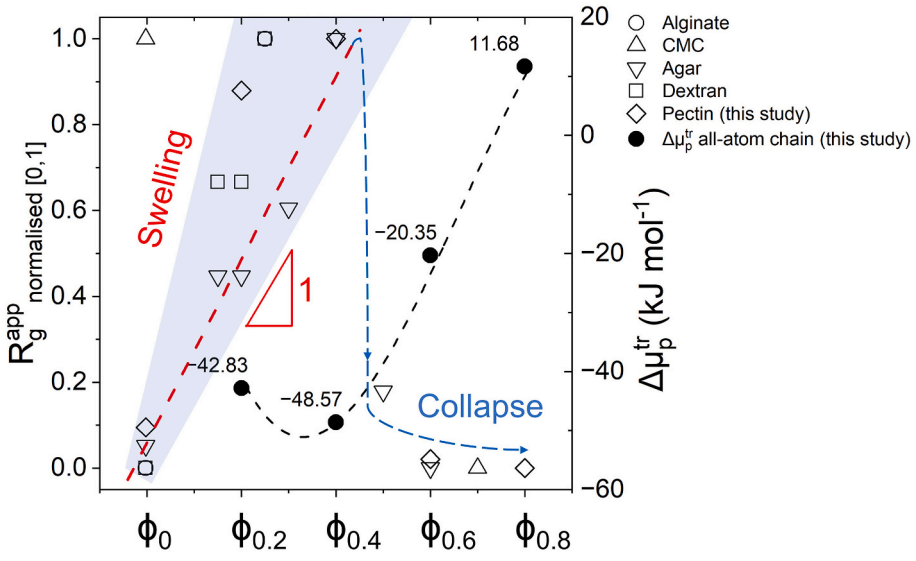

Fig. 7. Master comparison of apparent radius of gyration, R_g^{app} for various polysaccharides and transfer free energy, $\Delta\mu_p^{tr}$ from simulations plotted as a function of water-glycerol volume fraction ($\phi_{0-0.8}$). Experimental data for dextran, alginate, agar, and carboxymethylcellulose, are adapted from previous reports and is detailed in the manuscript. Blue region highlights the swelling and red dashed line is a power law fit for the agar data. Blue dashed line is a visual guide highlighting the collapse. Dashed black line is a cubic polynomial and used as a visual guide to highlight the transfer free energy, $\Delta\mu_p^{tr}$ derived using KB parameters. Readers should note that $\Delta\mu_p^{tr}$ is a pseudochemical potential which is roughly equivalent to the molar Gibbs free energy.

KB integrals as described earlier by Shimizu and Matubayasi (Shimizu & Matubayasi, 2024), gives us, $\left(\partial\mu_p^{tr}/\partial\mu_g\right)_{T,P,N_w} = -\rho_g(G_{pg}-G_{pw})$, where G_{pg} and G_{pw} are the KB integrals. As described earlier in this paper, the excess solvation number of glycerol molecules around the polysaccharide can be expressed as, $\Gamma_{pg}=\rho_g(G_{pg}-G_{pw})$ (Smiatek, 2017), thus implying that, $\left(\partial\mu_p^{tr}/\partial\mu_g\right)_{T,P,N_w} \propto -\Gamma_{pg}$. So, for a lower μ_p^{tr}, the relationship implies $\Gamma_{pg}>0$ corresponding to glycerol accumulation. In contrast, higher μ_p^{tr} implies $\Gamma_{pg}<0$ corresponding to glycerol exclusion and water enrichment in the polysaccharide's local environment, a solvent demixing which was captured experimentally in $\phi_{0.8}$ using dielectric spectroscopy. While this explains preferential solvation, it does not explain the conformational transitions and requires us to go beyond the KB description.

An important detail was uncovered in our simulations: the water accessible surface area of the polysaccharide chain showed a marked consistency across all solvent conditions (ca. 2% deviation), if compared to the notable ca. 10% changes in the end-to-end distance, $\overline{R}$ which captured the swelling and collapse (Fig. S8). Future investigations utilising low-field NMR relaxometry and contrast-variation small-angle neutron scattering may provide direct validation. Present simulations nevertheless suggest that a polysaccharide chain appears to conserve its total water contact by reconfiguring its conformation. At lower glycerol volume fraction, the polysaccharide chain experiences preferential binding of the poorer cosolvent, which depletes the chain of water. Under these conditions, water and glycerol subsystems lose entropy. Thus, the chain maximises its conformational entropy by adopting a more open (swollen) configuration. This is consistent with the increased ΔS_{conf} observed in $\phi_{0.4}$ from neutron scattering. Polymer solution theory (De Gennes, 1979) describes this observation as an increase in the effective attraction between monomers, which first brings polymer chains into a Θ-configuration as solvent quality deteriorates. In line, we estimated $c^*[\eta]^{app}$ for $\phi_{0.4}\approx 1$. Upon further increase of such attraction in a standard poor solvent, a polymer chain collapses into a compact configuration (Mukherji et al., 2017). On the contrary, at higher glycerol volume fraction ($\phi_{0.8}$), we observed that the polysaccharide exhibits preferential hydration. Here, the chain collapses even though the local environment is enriched with a good solvent. This cannot be rationalised using the standard definitions of polymer collapse in a poorer solvent. It is proposed that maintaining an exceedingly water-rich layer along the chain imposes an entropic penalty. By adopting a more compact conformation, the polysaccharide thus reduces its excess water contact. This solvent redistribution and gain in entropy for the water subpopulation make polysaccharide collapse thermodynamically favourable, even at the expense of chain conformational entropy. Our argument is consistent with the modest increase in ΔS_{hydr} observed for the localised water in $\phi_{0.8}$ from neutron scattering. While nanosegregation in water-glycerol mixtures has been reported previously (Alba-Simionesco et al., 2022), here the phenomenon appears to be greatly accentuated due to the disproportionately high complexity of the polysaccharide-water solvent accessible interface. In this sense, polysaccharides reshape the local solvent mixing and act as active participants in influencing solvent coordination around their chains, rather than passive objects immersed in a continuum solvent.

4. Conclusions and future perspectives

We conclude that preferential solvation of polysaccharide chains drives non-monotonic flexible coil → swollen → compact (collapsed) conformational transitions in binary mixtures of water and glycerol. Here, the relative balance between glycerol and water binding to the polysaccharide chain evolves from preferential binding of glycerol ($\phi_{0.2\to0.6}$) to preferential hydration of water ($\phi_{0.8}$). This behaviour mirrors the swelling and subsequent collapse of the polysaccharide chains. Our analysis of conformational entropic penalties suggests that the system balances its free energy through a mechanism in which the polysaccharide preserves its total contact with water by reconfiguring its conformation. From a thermodynamic perspective, the structural characteristics of polysaccharides may play a major role in determining the extent of their association with water (Gabius, 2018; Kaltner et al., 2019). Importantly, for the preferentially solvated water layer to incur an excess entropic penalty, which may comprise a single layer of water molecules in the first solvation shell (Russo et al., 2013), water molecules do not necessarily need to remain bound to the chains through hydrogen bonding. Instead, they may retain sufficient mobility to

undergo dynamic exchange with the bulk solvent. The only requirement is the preservation of the polysaccharide-water solvent accessible interface, which imposes marked constraints on the range of accessible conformations.

Our findings, together with the generalised comparison across pectin, agar, alginate, carboxymethylcellulose, and dextran, qualitatively suggest that this non-monotonic behaviour may be a common, or even a unified feature, for a broad range of polysaccharides in which preferential solvation occurs. In a biological context, this raises the possibility that living organisms may exploit this mechanism by accumulating poorer cosolvents to modify their intra- and extracellular environment. This could enable cells to regulate the conformational states of polysaccharide components and, consequently, the viscoelasticity of their cytosol, exopolysaccharide envelope, or cell walls. Such mechanisms could provide a physical basis for a range of polysaccharide-mediated functions, including plant cell wall assembly, mechanical integrity of biofilms, cellular signalling, and immunomodulation across diverse forms of life. From an industrial perspective, the proposed mechanism provides a foundation for novel strategies in the facile control of polysaccharide conformation and the design of responsive hydrogels beyond conventional classes of stimuli-responsive polymers. It may also open new avenues for improving the cold solubility and structuring of amylose (Tongbram et al., 2026; Zhu et al., 2025), thermoplastic behaviour of pectin (Gouveia et al., 2019), and functionality in carbohydrate-based foods, gels, synthetic plant and yeast cells, bioelectronics, and pharmaceuticals (Cao & Mezzenga, 2020; Paulraj et al., 2020; Pifferi et al., 2021; Zhong et al., 2011). Bridging biological and industrial opportunities, the present findings have the potential to advance the understanding of emerging carbohydrate behaviours, including folding-induced stiffness in polymeric carbohydrates (Anggara et al., 2021), modulation of reaction rates through altered energy barriers to reactant approach in preferentially solvated hyaluronan (Kutálková et al., 2021), and catalytic activity of 'glycan foldamers' (Liu & Delbianco, 2025). Our perspective should nevertheless be regarded as a working framework rather than a universal law. Several future research avenues could strengthen this framework. For example, simulations incorporating the full spectrum of polysaccharide architectural complexity under macromolecular crowding conditions may provide a molecular-level picture linking preferential solvation to concentration-dependent viscoelasticity. In parallel, experiments conducted at controlled ionic strength, including salt-screening and counterion-specific studies, will be important for disentangling preferential solvation effects from potential polyelectrolyte contributions. Several questions nevertheless remain open: How does preferential solvation affect the conformations of other homo- and heteropolysaccharides, such as amylose, guar gum, carrageenan, and pullulan? How does preferential solvation vary with temperature and pressure? How does it emerge in the presence of other poorer cosolvents? Regarding the latter question, and as noted in the introduction, the swelling and collapse of hyaluronic acid and alginate in miscible water-organic solvent mixtures containing 1,4-dioxane, tert-butanol, or ethanol, all of which are poorer cosolvents for these polysaccharides, have previously been observed (Hermansson et al., 2016; Kutálková et al., 2023). Such observations further support the tentatively unified nature of our proposed mechanism and suggest broad implications for both biological and industrial aspects of glycoscience.

CRediT authorship contribution statement

Pallab Kumar Borah: Writing – review & editing, Writing – original draft, Visualization, Validation, Software, Project administration, Methodology, Investigation, Funding acquisition, Formal analysis, Data curation, Conceptualization, Resources. **Joshua E.S.J. Reid:** Writing – review & editing, Validation, Methodology, Investigation, Formal analysis. **Thomas MacCalman:** Writing – review & editing, Validation, Methodology, Investigation, Formal analysis. **Amir H. Irani:** Writing – review & editing, Methodology, Investigation. **Daniela Russo:** Writing – review & editing, Methodology, Investigation. **Jens Smiatek:** Writing – review & editing, Software, Methodology, Investigation, Formal analysis. **Johannes Hunger:** Writing – review & editing, Software, Methodology, Investigation, Formal analysis, Resources. **Mona Sarter:** Writing – review & editing, Methodology, Formal analysis. **Vlad Dinu:** Writing – review & editing, Formal analysis. **Francesca Natali:** Writing – review & editing, Investigation. **Michael Boehm:** Writing – review & editing, Methodology. **Stephen E. Harding:** Writing – review & editing, Methodology, Resources. **Martin A.K. Williams:** Writing – review & editing, Methodology. **Stefan K. Baier:** Writing – review & editing, Methodology. **Gleb E. Yakubov:** Writing – review & editing, Supervision, Resources, Project administration, Methodology, Funding acquisition, Formal analysis, Conceptualization.

Declaration of competing interest

The authors declare that they have no competing interests that could have influenced the work reported in this paper.

Acknowledgement

PKB thanks funding received from the European Union's Horizon 2020 research and innovation programme under the Marie Skłodowska-Curie grant agreement No. 101034266. GEY thanks the Biotechnology and Biological Sciences Research Council (BBSRC Grant No. BB/T006404/1 and BB/W019639/1) for funding. All authors thank Motif FoodWorks Inc., USA, for part funding. PKB thanks Marcell Wolf and Adrian Stephan for providing flat aluminium cells and machining cell adapters for neutron experiments and Christopher J. Garvey for many useful discussions and help during experiments at the IN13 and IRIS neutron spectrometers (Beamtime Grant No. DIR-332 and RB2420353, respectively). PKB, JESJR, AHI, MAKW, and GEY acknowledge Seishi Shimizu, Vivek Sharma, Bianca Hazt, Xinxin Li, Benjamin Westberry, Philippe Prochasson, Reed Nicholson, and Lucas Kreuzer for useful discussions in solvation, extensional rheology, and Debye relaxation. PKB and AHI acknowledges the on-premises HPC services of Technical University of Munich and Waikato Hospital. PKB, DR, and FN acknowledges Leonardo Chiappisi and the Partnership for Soft Condensed Matter at Institute Laue-Langevin, France for access to calorimetry.

Appendix A. Supplementary data

Supplementary data to this article can be found online at https://doi.org/10.1016/j.carbpol.2026.125726.

Data availability

Simulation trajectories generated in this study are deposited to the Zenodo database under accession code: https://doi.org/10.5281/zenodo.18624448. Neutron scattering data are available at https://doi.org/10.5286/ISIS.E.RB2420353-1 and https://doi.org/10.5291/ILL-DATA.DIR-332. Any additional information can be made available from the corresponding authors upon reasonable request.

References

Ahn, Y., Kim, H., & Kwak, S.-Y. (2019). Self-reinforcement of alginate hydrogel via conformational control. *European Polymer Journal, 116*, 480–487. https://doi.org/10.1016/j.eurpolymj.2019.03.017

Alba, K., Bingham, R. J., Gunning, P. A., Wilde, P. J., & Kontogiorgos, V. (2018). Pectin conformation in solution. *The Journal of Physical Chemistry B, 122*(29), 7286–7294. https://doi.org/10.1021/acs.jpcb.8b04790

Alba-Simionesco, C., Judeinstein, P., Longeville, S., Osta, O., Porcher, F., Caupin, F., & Tarjus, G. (2022). Interplay of vitrification and ice formation in a cryoprotectant aqueous solution at low temperature. *Proceedings of the National Academy of Sciences*

of the United States of America, 119(12), Article e2112248119. https://doi.org/10.1073/pnas.2112248119
Anggara, K., Zhu, Y., Fittolani, G., Yu, Y., Tyrikos-Ergas, T., Delbianco, M., … Kern, K. (2021). Identifying the origin of local flexibility in a carbohydrate polymer. *Proceedings of the National Academy of Sciences of the United States of America, 118*(23), Article e2102168118. https://doi.org/10.1073/pnas.2102168118
Antoniou, E., & Alexandridis, P. (2010). Polymer conformation in mixed aqueous-polar organic solvents. *European Polymer Journal, 46*(2), 324–335. https://doi.org/10.1016/j.eurpolymj.2009.10.005
Arbe, A., Nilsen, G. J., Stewart, J. R., Alvarez, F., Sakai, V. G., & Colmenero, J. (2020). Coherent structural relaxation of water from meso- to intermolecular scales measured using neutron spectroscopy with polarization analysis. *Physical Review Research, 2*(2), Article 022015. https://doi.org/10.1103/PhysRevResearch.2.022015
Baran, K., Laugier, S., & Cramail, H. (1999). Investigation of molecular dimensions of polystyrene as a function of the solvent composition: Application to liquid chromatography at the exclusion-adsorption transition point. *Macromolecular Chemistry and Physics, 200*(9), 2074–2079. https://doi.org/10.1002/(SICI)1521-3935(19990901)200:9<2074::AID-MACP2074>3.0.CO;2-C
Batchelor, G. K. (1971). The stress generated in a non-dilute suspension of elongated particles by pure straining motion. *Journal of Fluid Mechanics, 46*(4), 813–829. https://doi.org/10.1017/S0022112071000879
Baynes, B. M., & Trout, B. L. (2003). Proteins in mixed solvents: A molecular-level perspective. *The Journal of Physical Chemistry B, 107*(50), 14058–14067. https://doi.org/10.1021/jp0363996
Berglund, J., Mikkelsen, D., Flanagan, B. M., Dhital, S., Gaunitz, S., Henriksson, G., … Vilaplana, F. (2020). Wood hemicelluloses exert distinct biomechanical contributions to cellulose fibrillar networks. *Nature Communications, 11*(1), 4692. https://doi.org/10.1038/s41467-020-18390-z
Bernal-Bayard, J., Thiebaud, J., Brossaud, M., Beaussart, A., Caillet, C., Waldvogel, Y., … Ghigo, J.-M. (2023). Bacterial capsular polysaccharides with antibiofilm activity share common biophysical and electrokinetic properties. *Nature Communications, 14*(1), 2553. https://doi.org/10.1038/s41467-023-37925-8
Boral, S., & Bohidar, H. B. (2012). Effect of water structure on gelation of agar in glycerol solutions and phase diagram of agar organogels. *The Journal of Physical Chemistry B, 116*(24), 7113–7121. https://doi.org/10.1021/jp3022024
Cao, Y., & Mezzenga, R. (2020). Design principles of food gels. *Nature Food, 1*(2), 106–118. https://doi.org/10.1038/s43016-019-0009-x
Charkhesht, A., Lou, D., Sindle, B., Wen, C., Cheng, S., & Vinh, N. Q. (2019). Insights into hydration dynamics and cooperative interactions in glycerol–water mixtures by terahertz dielectric spectroscopy. *The Journal of Physical Chemistry B, 123*(41), 8791–8799. https://doi.org/10.1021/acs.jpcb.9b07021
Davies, G. A., & Stokes, J. R. (2008). Thin film and high shear rheology of multiphase complex fluids. *Journal of Non-Newtonian Fluid Mechanics, 148*(1), 73–87. https://doi.org/10.1016/j.jnnfm.2007.04.013
Davies, G. A., & Stokes, J. R. (2005). On the gap error in parallel plate rheometry that arises from the presence of air when zeroing the gap. *Journal of Rheology, 49*(4), 919–922. https://doi.org/10.1122/1.1942501
De Gennes, P.-G. (1979). *Scaling concepts in polymer physics*. Cornell university press.
de Jong, J. C., McCormack, B. J., Smirnoff, N., & Talbot, N. J. (1997). Glycerol generates turgor in rice blast. *Nature, 389*(6648), 244. https://doi.org/10.1038/38418
Dinic, J., & Sharma, V. (2020). Power Laws dominate shear and extensional rheology response and capillarity-driven pinching dynamics of entangled hydroxyethyl cellulose (HEC) solutions. *Macromolecules, 53*(9), 3424–3437. https://doi.org/10.1021/acs.macromol.0c00077
Ditlecadet, D., Short, C. E., & Driedzic, W. R. (2010). Glycerol loss to water exceeds glycerol catabolism via glycerol kinase in freeze-resistant rainbow smelt (*Osmerus mordax*). *American Journal of Physiology, Regulatory, Integrative and Comparative Physiology, 300*(3), R674–R684. https://doi.org/10.1152/ajpregu.00700.2010
Ensing, W., Hunger, J., Ottosson, N., & Bakker, H. J. (2013). On the orientational mobility of water molecules in proton and sodium terminated Nafion membranes. *The Journal of Physical Chemistry C, 117*(25), 12930–12935. https://doi.org/10.1021/jp312623p
Finn, R. N., Chauvigné, F., Stavang, J. A., Belles, X., & Cerdà, J. (2015). Insect glycerol transporters evolved by functional co-option and gene replacement. *Nature Communications, 6*(1), 7814. https://doi.org/10.1038/ncomms8814
Fitter, J. (2003). A measure of conformational entropy change during thermal protein unfolding using neutron spectroscopy. *Biophysical Journal, 84*(6), 3924–3930. https://doi.org/10.1016/S0006-3495(03)75120-0
Freund, M., Graus, D., Fleischmann, A., Gilbert, K. J., Lin, Q., Renner, T., … Fukushima, K. (2022). The digestive systems of carnivorous plants. *Plant Physiology, 190*(1), 44–59. https://doi.org/10.1093/plphys/kiac232
Gabius, H.-J. (2018). The sugar code: Why glycans are so important. *Biosystems, 164*, 102–111. https://doi.org/10.1016/j.biosystems.2017.07.003
García de la Torre, J., & Hernández-Cifre, J. G. (2025). Hydrodynamic properties of macromolecules and nanoparticles in dilute solution: A brief essay on classical and modern concepts. *European Biophysics Journal, 54*(6), 331–349. https://doi.org/10.1007/s00249-025-01791-7
Gericke, M., Amaral, A. J. R., Budtova, T., De Wever, P., Groth, T., Heinze, T., … Fardim, P. (2024). The European Polysaccharide Network of Excellence (EPNOE) research roadmap 2040: Advanced strategies for exploiting the vast potential of polysaccharides as renewable bioresources. *Carbohydrate Polymers, 326*, Article 121633. https://doi.org/10.1016/j.carbpol.2023.121633
Gouveia, T. I. A., Biernacki, K., Castro, M. C. R., Gonçalves, M. P., & Souza, H. K. S. (2019). A new approach to develop biodegradable films based on thermoplastic pectin. *Food Hydrocolloids, 97*, Article 105175. https://doi.org/10.1016/j.foodhyd.2019.105175
Grant, O. C., Wentworth, D., Holmes, S. G., Kandel, R., Sehnal, D., Wang, X., … Woods, R. J. (2026). Generating 3D models of complex carbohydrates with GLYCAM-Web. *Nature Methods, 23*(4), 720–723. https://doi.org/10.1038/s41592-026-03033-w
Haas, K. T., Wightman, R., Meyerowitz, E. M., & Peaucelle, A. (2020). Pectin homogalacturonan nanofilament expansion drives morphogenesis in plant epidermal cells. *Science, 367*(6481), 1003–1007. https://doi.org/10.1126/science.aaz5103
Harding, S. E., Rowe, A. J., & Creeth, J. M. (1983). Further evidence for a flexible and highly expanded spheroidal model for mucus glycoproteins in solution. *Biochemical Journal, 209*(3), 893–896. https://doi.org/10.1042/bj2090893
Haydukivska, K., Blavatska, V., & Paturej, J. (2020). Universal size ratios of Gaussian polymers with complex architecture: Radius of gyration vs hydrodynamic radius. *Scientific Reports, 10*(1), 14127. https://doi.org/10.1038/s41598-020-70649-z
Hermansson, E., Schuster, E., Lindgren, L., Altskär, A., & Ström, A. (2016). Impact of solvent quality on the network strength and structure of alginate gels. *Carbohydrate Polymers, 144*, 289–296. https://doi.org/10.1016/j.carbpol.2016.02.069
Hernandez-Tamargo, C., Silverwood, I. P., O'Malley, A. J., & Leeuw, N. H.d. (2021). Quasielastic neutron scattering and molecular dynamics simulation study on the molecular behaviour of catechol in zeolite beta. *Topics in Catalysis, 64*(9), 707–721. https://doi.org/10.1007/s11244-020-01400-1
Jimenez, L. N., Martínez Narváez, C. D. V., & Sharma, V. (2020). Capillary breakup and extensional rheology response of food thickener cellulose gum (NaCMC) in salt-free and excess salt solutions. *Physics of Fluids, 32*(1), Article 012113. https://doi.org/10.1063/1.5128254
Jimenez, L. N., Martínez Narváez, C. D. V., & Sharma, V. (2022). Solvent properties influence the rheology and pinching dynamics of polyelectrolyte solutions: Thickening the pot with glycerol and cellulose gum. *Macromolecules, 55*(18), 8117–8132. https://doi.org/10.1021/acs.macromol.2c00170
Kaltner, H., Abad-Rodríguez, J., Corfield, A. P., Kopitz, J., & Gabius, H.-J. (2019). The sugar code: Letters and vocabulary, writers, editors and readers and biosignificance of functional glycan–lectin pairing. *Biochemical Journal, 476*(18), 2623–2655. https://doi.org/10.1042/BCJ20170853
Kirschner, K. N., Yongye, A. B., Tschampel, S. M., González-Outeiriño, J., Daniels, C. R., Foley, B. L., & Woods, R. J. (2008). GLYCAM06: A generalizable biomolecular force field. Carbohydrates [doi:10.1002/jcc.20820]. *Journal of Computational Chemistry, 29*(4), 622–655. https://doi.org/10.1002/jcc.20820
Krüger, P., Schnell, S. K., Bedeaux, D., Kjelstrup, S., Vlugt, T. J. H., & Simon, J.-M. (2013). Kirkwood–Buff integrals for finite volumes. *The Journal of Physical Chemistry Letters, 4*(2), 235–238. https://doi.org/10.1021/jz301992u
Kumar, P., Yan, Z., Xu, L., Mazza, M. G., Buldyrev, S. V., Chen, S. H., … Stanley, H. E. (2006). Glass transition in biomolecules and the liquid-liquid critical point of water. *Physical Review Letters, 97*(17), Article 177802. https://doi.org/10.1103/PhysRevLett.97.177802
Kutálková, E., Hrnčiřík, J., Witasek, R., Ingr, M., Huerta-Ángeles, G., Hermannová, M., & Velebný, V. (2021). The rate and evenness of the substitutions on hyaluronan grafted by dodecanoic acid influenced by the mixed-solvent composition. *International Journal of Biological Macromolecules, 189*, 826–836. https://doi.org/10.1016/j.ijbiomac.2021.08.137
Kutálková, E., Ingr, M., Kolaříková, A., Hrnčiřík, J., Witasek, R., Hermannová, M., … Huerta-Ángeles, G. (2023). Structure and dynamics of the hyaluronan oligosaccharides and their solvation shell in water: Organic mixed solvents. *Carbohydrate Polymers, 304*, Article 120506. https://doi.org/10.1016/j.carbpol.2022.120506
Le Pennec, J., Makshakova, O., Nevola, P., Fouladkar, F., Gout, E., Machillot, P., … Migliorini, E. (2024). Glycosaminoglycans exhibit distinct interactions and signaling with BMP2 according to their nature and localization. *Carbohydrate Polymers, 341*, Article 122294. https://doi.org/10.1016/j.carbpol.2024.122294
Li, X., Harding, S. E., Wolf, B., & Yakubov, G. E. (2022). Instrumental characterization of xanthan gum and scleroglucan solutions: Comparison of rotational rheometry, capillary breakup extensional rheometry and soft-contact tribology. *Food Hydrocolloids, 130*, Article 107681. https://doi.org/10.1016/j.foodhyd.2022.107681
Litvinova, L., & Bel'nikevich, N. (2003). Adsorption thin-layer chromatography and viscometry of polystyrenes in solvent mixtures. *Journal of Chromatography A, 1005*(1), 165–176. https://doi.org/10.1016/S0021-9673(03)00844-6
Liu, K., & Delbianco, M. (2025). A glycan foldamer that uses carbohydrate–aromatic interactions to perform catalysis. *Nature Chemistry, 17*(6), 883–889. https://doi.org/10.1038/s41557-025-01763-6
Manrique, G. D., & Lajolo, F. M. (2002). FT-IR spectroscopy as a tool for measuring degree of methyl esterification in pectins isolated from ripening papaya fruit. *Postharvest Biology and Technology, 25*(1), 99–107. https://doi.org/10.1016/S0925-5214(01)00160-0
Mao, Y., Millett, R., Lee, C. S., Yakubov, G., Harding, S. E., & Binner, E. (2020). Investigating the influence of pectin content and structure on its functionality in bio-flocculant extracted from okra. *Carbohydrate Polymers, 241*, Article 116414. https://doi.org/10.1016/j.carbpol.2020.116414
Marth, J. D. (2008). A unified vision of the building blocks of life. *Nature Cell Biology, 10*(9), 1015. https://doi.org/10.1038/ncb0908-1015
Mazur, K., Buchner, R., Bonn, M., & Hunger, J. (2014). Hydration of sodium alginate in aqueous solution. *Macromolecules, 47*(2), 771–776. https://doi.org/10.1021/ma4023873
Milzetti, J., Nayar, D., & van der Vegt, N. F. A. (2018). Convergence of Kirkwood–Buff integrals of ideal and nonideal aqueous solutions using molecular dynamics

simulations. *The Journal of Physical Chemistry B, 122*(21), 5515–5526. https://doi.org/10.1021/acs.jpcb.7b11831
Miyazaki, Y., Matsuo, T., & Suga, H. (2000). Low-temperature heat capacity and glassy behavior of lysozyme crystal. *The Journal of Physical Chemistry B, 104*(33), 8044–8052. https://doi.org/10.1021/jp0007686
Morris, G. A., Ralet, M.-C., Bonnin, E., Thibault, J.-F., & Harding, S. E. (2010). Physical characterisation of the rhamnogalacturonan and homogalacturonan fractions of sugar beet (Beta vulgaris) pectin. *Carbohydrate Polymers, 82*(4), 1161–1167. https://doi.org/10.1016/j.carbpol.2010.06.049
Mukherji, D., Marques, C. M., & Kremer, K. (2014). Polymer collapse in miscible good solvents is a generic phenomenon driven by preferential adsorption. *Nature Communications, 5*(1), 4882. https://doi.org/10.1038/ncomms5882
Mukherji, D., Marques, C. M., Stuehn, T., & Kremer, K. (2017). Depleted depletion drives polymer swelling in poor solvent mixtures. *Nature Communications, 8*(1), 1374. https://doi.org/10.1038/s41467-017-01520-5
Nakagawa, H., & Oyama, T. (2019). Molecular basis of water activity in glycerol–water mixtures [original research]. *Frontiers in Chemistry, 7*. https://doi.org/10.3389/fchem.2019.00731
Nalam, P. C., Ramakrishna, S. N., Espinosa-Marzal, R. M., & Spencer, N. D. (2013). Exploring lubrication regimes at the nanoscale: Nanotribological characterization of silica and polymer brushes in viscous solvents. *Langmuir, 29*(32), 10149–10158. https://doi.org/10.1021/la402148b
Paulraj, T., Wennmalm, S., Wieland, D. C. F., Riazanova, A. V., Dėdinaitė, A., Günther Pomorski, T., … Svagan, A. J. (2020). Primary cell wall inspired micro containers as a step towards a synthetic plant cell. *Nature Communications, 11*(1), 958. https://doi.org/10.1038/s41467-020-14718-x
Pifferi, C., Fuentes, R., & Fernández-Tejada, A. (2021). Natural and synthetic carbohydrate-based vaccine adjuvants and their mechanisms of action. *Nature Reviews Chemistry, 5*(3), 197–216. https://doi.org/10.1038/s41570-020-00244-3
Pincus, I., Rodger, A., & Prakash, J. R. (2020). Viscometric functions and rheo-optical properties of dilute polymer solutions: Comparison of FENE-Fraenkel dumbbells with rodlike models. *Journal of Non-Newtonian Fluid Mechanics, 285*, Article 104395. https://doi.org/10.1016/j.jnnfm.2020.104395
Raymond, J. A., Morgan-Kiss, R., & Stahl-Rommel, S. (2020). Glycerol is an osmoprotectant in two Antarctic Chlamydomonas species from an ice-covered saline lake and is synthesized by an unusual bidomain enzyme [original research]. *Frontiers in Plant Science, 11*. https://doi.org/10.3389/fpls.2020.01259
Rinne, K. F., Gekle, S., & Netz, R. R. (2014). Ion-specific solvation water dynamics: Single water versus collective water effects. *The Journal of Physical Chemistry A, 118*(50), 11667–11677. https://doi.org/10.1021/jp5066874
Rivlin, R. S. (1948). Normal stress coefficient in solutions of macromolecules. *Nature, 161*(4093), 567–568. https://doi.org/10.1038/161567a0
Russo, D., Gonzalez, M. A., Pellegrini, E., Combet, J., Ollivier, J., & Teixeira, J. (2013). Evidence of dynamical constraints imposed by water organization around a bio–hydrophobic interface. *The Journal of Physical Chemistry B, 117*(10), 2829–2836. https://doi.org/10.1021/jp3094885
Russo, D., & Teixeira, J. (2015). Mapping water dynamics in defined local environment: From hindered rotation to vibrational modes. *Journal of Non-Crystalline Solids, 407*, 459–464. https://doi.org/10.1016/j.jnoncrysol.2014.07.030
Sabbadin, F., Hemsworth, G. R., Ciano, L., Henrissat, B., Dupree, P., Tryfona, T., … McQueen-Mason, S. J. (2018). An ancient family of lytic polysaccharide monooxygenases with roles in arthropod development and biomass digestion. *Nature Communications, 9*(1), 756. https://doi.org/10.1038/s41467-018-03142-x
Sarter, M., Stewart, J. R., Nilsen, G. J., Devonport, M., & Nemkovski, K. (2024). Data analysis of dynamics in protein solutions using quasi-elastic neutron scattering—Important insights from polarized neutrons. *Journal of the American Chemical Society, 146*(41), 28023–28033. https://doi.org/10.1021/jacs.4c06273
Shimizu, S., & Matubayasi, N. (2024). Synergistic solvation as the enhancement of local mixing. *The Journal of Physical Chemistry B, 128*(23), 5713–5726. https://doi.org/10.1021/acs.jpcb.4c01582
Smiatek, J. (2017). Aqueous ionic liquids and their effects on protein structures: An overview on recent theoretical and experimental results. *Journal of Physics: Condensed Matter, 29*(23), Article 233001. https://doi.org/10.1088/1361-648X/aa6c9d
Spellmon, N., Muszyński, A., Górniak, I., Vlach, J., Hahn, D., Azadi, P., & Zimmer, J. (2022). Molecular basis for polysaccharide recognition and modulated ATP hydrolysis by the O antigen ABC transporter. *Nature Communications, 13*(1), 5226. https://doi.org/10.1038/s41467-022-32597-2
Stadler, A. M., Koza, M. M., & Fitter, J. (2015). Determination of conformational entropy of fully and partially folded conformations of holo- and apomyoglobin. *The Journal of Physical Chemistry B, 119*(1), 72–82. https://doi.org/10.1021/jp509732q
Stelter, M., Brenn, G., Yarin, A. L., Singh, R. P., & Durst, F. (2002). Investigation of the elongational behavior of polymer solutions by means of an elongational rheometer. *Journal of Rheology, 46*(2), 507–527. https://doi.org/10.1122/1.1445185
Swenson, J., Bergman, R., & Howells, W. S. (2000). Quasielastic neutron scattering of two-dimensional water in a vermiculite clay. *The Journal of Chemical Physics, 113*(7), 2873–2879. https://doi.org/10.1063/1.1305870
Tongbram, T., Vaniyan, L., MacCalman, T., Bharati, A., Warren, F. J., Badwaik, L. S., … Yakubov, G. E. (2026). Soluble amylose chains inhibit gelatinisation and retrogradation in waxy corn starch. *Food Hydrocolloids, 172*, Article 111936. https://doi.org/10.1016/j.foodhyd.2025.111936
Toxopeus, J., Koštál, V., & Sinclair, B. J. (2019). Evidence for non-colligative function of small cryoprotectants in a freeze-tolerant insect. *Proceedings of the Royal Society B: Biological Sciences, 286*(1899), Article 20190050. https://doi.org/10.1098/rspb.2019.0050
Vaniyan, L., Borah, P. K., Pavlovskaya, G. E., Terrill, N., Reid, J. E. S. J., Boehm, M., … Yakubov, G. E. (2025). Wet spinning of sodium carboxymethyl cellulose–sodium caseinate hydrogel fibres: Relationship between rheology and spinnability [10.1039/D4SM00705K]. *Soft Matter, 21*(20), 3946–3956. https://doi.org/10.1039/D4SM00705K
Wachsman, G., Zhang, J., Moreno-Risueno, M. A., Anderson, C. T., & Benfey, P. N. (2020). Cell wall remodeling and vesicle trafficking mediate the root clock in Arabidopsis. *Science, 370*(6518), 819–823. https://doi.org/10.1126/science.abb7250
Wang, A., Breakwell, C., Foglia, F., Tan, R., Lovell, L., Wei, X., … Song, Q. (2024). Selective ion transport through hydrated micropores in polymer membranes. *Nature, 635*(8038), 353–358. https://doi.org/10.1038/s41586-024-08140-2
Yuan, B., Ritzoulis, C., & Chen, J. (2018). Extensional and shear rheology of okra polysaccharides in the presence of artificial saliva. *npj Science of Food, 2*(1), Article 20. https://doi.org/10.1038/s41538-018-0029-1
Zaccai, G. (2000). How soft is a protein? A protein dynamics force constant measured by neutron scattering. *Science, 288*(5471), 1604–1607. https://doi.org/10.1126/science.288.5471.1604
Zdunek, A., Pieczywek, P. M., & Cybulska, J. (2021). The primary, secondary, and structures of higher levels of pectin polysaccharides [doi:10.1111/1541-4337.12689]. *Comprehensive Reviews in Food Science and Food Safety, 20*(1), 1101–1117. https://doi.org/10.1111/1541-4337.12689
Zhang, G., & Wu, C. (2001). The water/methanol complexation induced reentrant coil-to-globule-to-coil transition of individual homopolymer chains in extremely dilute solution. *Journal of the American Chemical Society, 123*(7), 1376–1380. https://doi.org/10.1021/ja003889s
Zhao, Y., Liu, M., He, L., Li, X., Wang, F., Yan, B., Wei, J., Zhao, C., Li, Z., & Xu, J. (2019). A cytosolic NAD+-dependent GPDH from maize (ZmGPDH1) is involved in conferring salt and osmotic stress tolerance. *BMC Plant Biology, 19*(1), 16. https://doi.org/10.1186/s12870-018-1597-6
Zhong, C., Deng, Y., Roudsari, A. F., Kapetanovic, A., Anantram, M. P., & Rolandi, M. (2011). A polysaccharide bioprotonic field-effect transistor. *Nature Communications, 2*(1), 476. https://doi.org/10.1038/ncomms1489
Zhu, Z., Yu, Y., Yu, Z., Xu, Y., Du, X., & Chen, X. (2025). Structure-stabilizing effect of glycerol on amylose promotes the formation of V-type starch with controlled digestibility. *Carbohydrate Polymers, 366*, Article 123865. https://doi.org/10.1016/j.carbpol.2025.123865
Znamenskaya, Y., Sotres, J., Engblom, J., Arnebrant, T., & Kocherbitov, V. (2012). Effect of hydration on structural and thermodynamic properties of pig gastric and bovine submaxillary gland mucins. *The Journal of Physical Chemistry B, 116*(16), 5047–5055. https://doi.org/10.1021/jp212495t